Functions of the *Dictyostelium* LIMP-2/CD36 homologues in bacteria uptake, phagolysosome biogenesis and host cell defence

Natascha Sattler[1&], Cristina Bosmani[1&], Caroline Barisch[1], Aurélie Guého[1], Navin Gopaldass[1,4], Marco Dias[3], Florence Leuba[1], Franz Bruckert[2], Pierre Cosson[3], and Thierry Soldati[1]*

[1]Départment de Biochimie, Faculté des Sciences, Université de Genève, Sciences II, 30 quai Ernest Ansermet, CH-1211 Genève-4, Switzerland

[2]Laboratoire des Matériaux et du Génie Physique (LMGP), Grenoble Institute of Technology, 3 parvis Louis Néel, BP 257, 38016 Grenoble cedex 1, France

[3]Department of Cell Physiology and Metabolism, Centre Médical Universitaire, University of Geneva, 1 rue Michel Servet, CH-1211 Geneva 4, Switzerland.

[4]Current address: Département de Biochimie, Faculté des Sciences, Université Lausanne, Chemin des Boveresses 155 CH-1066 Epalinges, Switzerland

[&]These authors contributed equally

*Corresponding author

Thierry.Soldati@unige.ch

Tel: +41-22-379- 6496

Fax: +41-22-379-3499

JCS Advance Online Article. Posted on 27 July 2018

Abstract

Phagocytic cells take up, kill and digest microbes by a process called phagocytosis. To this end these cells bind the particle, rearrange their actin cytoskeleton, and orchestrate transport of digestive factors to the particle-containing phagosome. The mammalian lysosomal membrane protein LIMP-2 and CD36, members of the class B of scavenger receptors, play a crucial role in lysosomal enzyme trafficking and uptake of mycobacteria, respectively, and generally in host cell defences against intracellular pathogens. Here, we show that the *Dictyostelium discoideum* LIMP-2 homologue LmpA regulates phagocytosis and phagolysosome biogenesis. The *lmpA* knockdown mutant is highly affected in actin-dependent processes such as particle uptake, cellular spreading and motility. Additionally, the cells are severely impaired in phagosomal acidification and proteolysis, likely explaining the higher susceptibility to infection with the pathogenic bacterium *Mycobacterium marinum*, a close cousin of the human pathogen *Mycobacterium tuberculosis*. Furthermore, we bring evidence that LmpB is a functional homologue of CD36 and specifically mediates uptake of mycobacteria. Altogether, these data indicate a role for LmpA and LmpB, ancestors of the LIMP-2/CD36 family, in lysosome biogenesis and host cell defence.

Summary Statement: *Dictyostelium discoideum* LmpA and LmpB are functional homologues of LIMP-2 and CD36, respectively, and play roles in phagosome maturation and host defence against a bacterial pathogen

Keywords: phagocytosis / phagosome maturation / *Dictyostelium discoideum* / CD36 / LIMP-2 / mycobacteria

Introduction

Phagocytic cells of our immune system take up particles larger than 250 nm in diameter by phagocytosis and are the first line of defence against pathogens. Originally developed by early eukaryotes for nutrition purposes, phagocytosis was fine-tuned by immune phagocytes to take up pathogens, kill them and activate immune responses. The mechanisms of phagocytosis and digestion of bacteria are extremely conserved (Boulais et al., 2010; Dunn et al., 2017), and therefore, the social amoeba *Dictyostelium discoideum* is, with its haploid genome and easy genetic and biochemical accessibility, a versatile experimental model organism to study these processes (Boulais et al., 2010; Bozzaro et al., 2008; Cosson and Soldati, 2008; Maniak, 2003). In addition, *D. discoideum* also emerged as a powerful system to study bacterial capture and killing, as well as host-pathogen interactions (Cosson and Lima, 2014; Cosson and Soldati, 2008; Dunn et al., 2017), especially as infection model for human pathogens such as *Legionella*, *Klebsiella*, *Mycobacterium*, *Pseudomonas* [reviewed in (Alibaud et al., 2008; Cardenal-Munoz et al., 2017; Hagele et al., 2000; Lelong et al., 2011; Solomon et al., 2003; Steinert and Heuner, 2005; Swart et al., 2018)], *Vibrio cholera* (Miyata et al., 2011), *Salmonella enterica* serovar Typhimurium (Jia et al., 2009) and fungi such as *Cryptococcus neoformans* (Fuchs and Mylonakis, 2006) and *Candida albicans* (Koller et al., 2016).

Phagocytes bind particles via surface receptors. While some receptors recognize opsonized particles, pattern recognition receptors (PRRs) bind to pathogen-associated molecular patterns (PAMPs). PRRs include C-type lectins, Toll-like receptors and the scavenger receptor class B members CD36 and SR-B. This protein family is known to recognize anionic phospholipids of endogenous origin, but is also important for the uptake of specific pathogens [(Neculai et al., 2013), for review see (Silverstein and Febbraio, 2009)]. In particular, scavenger receptors of class B have been implicated in the phagocytosis of mycobacteria (Areschoug and Gordon, 2009; Court et al., 2010; Philips et al., 2005; Schafer et al., 2009). The type III transmembrane proteins CD36, SR-B and the lysosomal integral membrane protein type 2 (LIMP-2) belong to class B. They have N- and C-terminal transmembrane domains, inducing a hairpin structure with a large glycosylated extracellular loop [reviewed in (Silverstein and Febbraio, 2009)]. While CD36 and SR-B are found in lipid rafts at the plasma membrane (Triantafilou et al., 2006), LIMP-2 is only present in endosomes (Vega et al., 1991). These proteins are highly conserved and expressed in diverse organisms such as phagocytic protozoans, sponges, worms, insects and mammals. They mediate uptake of various microbes such as fungi, Gram-positive and -negative bacteria, and mycobacteria (Baranova et al.,

2010; Baranova et al., 2008; Court et al., 2010; Philips et al., 2005; Schafer et al., 2009; Stuart et al., 2005; Vishnyakova et al., 2006). The C-terminal cytosolic tail of human CD36 plays a particular role, since mutation of tyrosine 463 causes a severe decrease in the phagocytosis of *Staphylococcus aureus* (Stuart et al., 2005). In addition, absence of CD36 in mice and worms leads to high susceptibility to infection with pathogenic *S. aureus* or *C. neoformans,* and to impairment in clearing pathogens (Hoebe et al., 2005; Means et al., 2009; Stuart et al., 2005).

Binding to phagocytic receptors triggers reorganization of the actin cytoskeleton to form a cup, enclosing the particle in a *de novo* compartment called phagosome, with contributions from the plasma membrane, the endoplasmic reticulum (ER) and endosomes (Dieckmann et al., 2012). The newly formed organelle is transiently coated with actin (Dieckmann et al., 2012; Liebl and Griffiths, 2009), but a series of fusion and fission events ensure maturation of the phagosome into a digestive organelle, the lysosome (Soldati and Neyrolles, 2012). In the lysosome, the production of reactive oxygen species (ROS) by the NADPH-oxidase complex (Zhang and Soldati, 2013), the drop in pH caused by the vacuolar H^+-ATPase (vATPase) (Aubry et al., 1993; Clarke et al., 2002; Clarke et al., 2010; Gotthardt et al., 2006a; Gotthardt et al., 2002), and the delivery of intoxicating metal ions and hydrolases kill and degrade the ingested pathogen (Dunn et al., 2017; Soldati and Neyrolles, 2012). In mammalian cells, most lysosomal enzymes are transported from the Golgi to the endosomes via the mannose-6-phosphate receptors (MPR). However, β-glucocerebrosidase is delivered to endosomes by LIMP-2 (Blanz et al., 2010; Blanz et al., 2015; Reczek et al., 2007). LIMP-2 [formerly known as LPG-85 (Kuronita et al., 2002; Kuronita et al., 2005)] belongs to the CD36 family of scavenger receptors. It is required for the biogenesis and maintenance of lysosomes and endosomes (Gonzalez et al., 2014), and regulates phagosome-lysosome fusion (Carrasco-Marin et al., 2011). Its absence decreases the proteolytic killing ability of the phagosome, leading to a higher susceptibility to infection with *Listeria monocytogenes* (Carrasco-Marin et al., 2011).

Pathogenic mycobacteria have evolved ways to circumvent the bactericidal milieu of the phagosome (Haas, 2007). The causative agent of tuberculosis, *M. tuberculosis*, inhibits phagosome maturation by preventing fusion of phagosomes with endosomal compartments and lysosomes (Sturgill-Koszycki et al., 1994; Vergne et al., 2004). By manipulating phagosomal maturation and the host cell autonomous defence, the bacteria create a permissive niche in which they multiply. Eventually, *M. tuberculosis* escapes from the phagosome as a consequence of the secretion of ESAT-6, a membranolytic

peptide (Simeone et al., 2011) that cooperates with phthiocerol dimycocerosates (Augenstreich et al., 2017) to damage the limiting membrane (Simeone et al., 2015). These steps of the life cycle are extremely similar to the ones documented for *M. marinum*, which bears a high level of similarity with *M. tuberculosis*, but infects fish and frogs and induces granulomatous lesions that are comparable to those found in human tuberculosis patients (Hagedorn and Soldati, 2009; Ramakrishnan et al., 2000; Swaim et al., 2006). *D. discoideum* has been established as an alternative model to study mechanisms of *M. marinum* infection at cellular and molecular levels (Arafah et al., 2013; Barisch et al., 2015; Cardenal-Munoz et al., 2017; Hagedorn et al., 2009; Hagedorn and Soldati, 2007). Because of its life style as a bacteria-hunting phagocyte, it is expected that phagocytic receptors are numerous and redundant in this soil-dwelling amoeba. Signature sequences of receptors, such as several peptidoglycan-binding LysM-motifs, leucine-rich repeats (LRR) and domains of C-type lectins, EGF/laminin and mannose-6-phosphate receptors (Eichinger et al., 2005), have been identified *in silico*. Several of these proteins were found at the plasma membrane and therefore suggested to take part in cell adhesion and signalling (Eichinger et al., 2005). Yet, only few cell surface receptors have been functionally described. Recently, the folic acid and G-protein coupled receptor fAR1 was shown to mediate chemotaxis towards bacterially-secreted folate and phagocytosis of the bacteria (Pan et al., 2016). In addition, the receptors SibA and SibC (similar to integrin-beta A and C), which are homologues of mammalian β-integrins, play a role during cell adhesion and phagocytosis (Cornillon et al., 2008; Cornillon et al., 2006; Froquet et al., 2012).

D. discoideum possesses three LIMP-2/CD36 family members: the lysosomal membrane glycoprotein LmpA (formerly known as DdLIMP-2), LmpB (formerly known as DdCD36) and LmpC (Harris et al., 2001a; Harris et al., 2001b; Karakesisoglou et al., 1999). LmpB localizes to lipid rafts of the plasma membrane and early phagosomes in a way comparable to CD36 and SR-B (Buckley et al., 2016; Gotthardt et al., 2006a; Gotthardt et al., 2002; Harris et al., 2001a; Harris et al., 2001b; Silverstein and Febbraio, 2009). On the other hand, LmpA and LmpC, like LIMP-2, are found in endosomes and lysosomes, and LmpA was postulated to participate in endosomal trafficking (Karakesisoglou et al., 1999; Temesvari et al., 2000). Knock down of the latter not only decreases fluid phase exocytosis but also impairs fluid phase acidification (Temesvari et al., 2000). Additionally, it was shown that LmpA binds to negatively charged phosphatidylinositides such as $PI(4,5)P_2$ with a putative ICAM-like binding domain (Karakesisoglou et al., 1999). Interestingly, neither LmpB nor LmpC possess this domain (Janssen et al., 2001). Both, LmpA and

LmpC have the typical LAMP-1 sorting motif GYXXΦ, while LmpB has two di-leucine sorting motifs, as seen in LIMP-2. The domains and motifs present in LmpA, LmpB and LmpC might explain their differential distribution in the cell [a drawing of their predicted structure is presented in Figure 2 of (Janssen et al., 2001)].

Here, we comprehensively study the three *D. discoideum* homologues of the mammalian scavenger receptors class B family and show that LmpA is an important factor involved in phagocytosis, lysosomal biogenesis and resistance to mycobacterial infection, while LmpB's function appears restricted to the uptake of mycobacteria and *B. subtilis*.

Results

LmpA and LmpC share the closest homology and were detected in the endophagosomal compartments, whereas LmpB is at the cell surface (Gotthardt et al., 2002). To confirm these results, surface proteins were biotinylated and pulled-down on avidin-coated beads. Isolated fractions were analysed by immunoblotting (Fig. 1A). As previously reported, the integrin-like protein SibA (Cornillon et al., 2006) and the glycoprotein GP130 (Chia, 1996) were enriched in the plasma membrane fraction. As expected, LmpB was found at the cell surface, albeit with a lower enrichment than SibA and GP130, suggesting that it is also present in endososomal compartments (see also Fig. 6B). LmpA was not detected in the plasma membrane fraction, confirming that this protein is exclusively found in endosomes, as previously suggested (Gotthardt et al., 2002). The expression level of LmpC is too low to allow detection in this experiment, but it was previously detected in purified phagosomal compartments (see below Fig. 6B). To visualize LmpA and LmpB in cells, we generated a *lmpA* knock down (kd) *D. discoideum* strain expressing LmpA-FLAG and a wild-type (wt) *D. discoideum* strain expressing LmpB-FLAG (Fig. 1B-D). The levels of expression of LmpA-FLAG and LmpB-FLAG were adjusted with doxycycline to be similar to the endogenous proteins, and the localizations of LmpA-FLAG and LmpB-FLAG during maturation of phagosomes containing latex beads (BCP) was studied by immunofluorescence (Fig. 1B-D). LmpA-FLAG was not present at the plasma membrane and was detected on a fraction of early phagosomes (15 min after uptake) and phagolysosomes 45 min after uptake, Fig. 1C). LmpA-FLAG was found in phagosomes mainly after 90 minutes (Fig. 1C) and colocalized with the predicted copper transporter p80, a marker of lysosomes and postlysosomes. This result corroborates the temporal profile of endogenous LmpA obtained from purified phagosomes (Gotthardt et

al., 2006a; Gotthardt et al., 2002). In contrast to LmpA-FLAG, LmpB-FLAG was localised in patches at the plasma membrane and the forming BCP (Fig. 1D). Overall, our data corroborate that LmpB is at the plasma membrane and in early endosomes, while LmpA and LmpC are absent from the surface and only found at later stages of maturation of phagosomal compartments, as summarized in Fig. 1E.

The lmpA kd and *lmpB* ko cells are defective in phagocytic uptake

Scavenger receptors of class B can mediate entry of microbes into host cells. In order to assess a possible function of the LmpA/B/C paralogs during uptake, flow cytometry assays were performed using a range of fluorescent particles such as 1 µm latex beads and Alexa-488-stained or GFP-producing representatives of Gram-positive (*Bacillus subtilis*) and negative (*K. pneumoniae*) bacteria, as well as *M. marinum* wt, the avirulent *M. marinum* mutant L1D (Ramakrishnan et al., 2000), and the non-pathogenic *M. smegmatis* (Fig. 2). The *lmpA* kd cells showed uptake defects for all particles tested. These cells phagocytosed 60–70% less beads and *K. pneumoniae*, and 80 – 90% less *M. smegmatis* and *B. subtilis* than wt cells. While the initial uptake rates for *K. pneumoniae* and *B. subtilis* were reduced 4.0- and 6.5-fold, respectively, the most significant reduction was observed for *M. smegmatis*, with a 20-fold decrease compared to wt cells (Fig. 2A-F). These results indicate that the *lmpA* kd defect in particle uptake depends on the nature of the particle, and is more drastic than the defect in fluid phase uptake (Sup. Fig. 1A). Compared to the general uptake defect in the *lmpA* kd, *lmpB* knock-out (ko) cells were severely impaired in the phagocytosis of all the mycobacterial strains tested as well as the Gram-positive bacterium *B. subtilis*. Ingestion of *M. marinum* wt, L1D and *B. subtilis* was around 40% lower, with an even stronger reduction of 60% for *M. smegmatis*. Nevertheless, the uptake was never as impaired as in the *lmpA* kd strain. Finally, the initial uptake rate in wt and *lmpC* ko cells was similar for the particles tested (1.9 - 2.7 relative fluorescent units (RFU)/min for wt and 1.6 - 2.3 RFU/min for *lmpC* ko cells), with a steady state reached after 60 min in most cases, except for ingestion of *M. marinum* wt, which was decreased by 20% (Fig. 2E).

Overall, these findings suggest that LmpA plays a major and as of yet unrecognized role during phagocytic uptake, with some degree of specificity towards Gram-positive bacteria and mycobacteria, while LmpB is specifically important for the phagocytic uptake of mycobacteria and possibly Gram-positive bacteria.

Cell surface levels of SibA and LmpB are altered in the *lmpA* kd, *lmpB* ko and *lmpC* ko mutants

The uptake phenotypes (Fig. 2), together with the localisation data (Fig. 1), led us to hypothesize that surface LmpB might serve as a phagocytic receptor, while endolysosomal LmpA and LmpC might influence receptor trafficking. To test this hypothesis, the surface of the *D. discoideum* strains was biotinylated, and their plasma membrane proteins were isolated. The distribution of LmpB and the phagocytic receptor SibA was monitored by quantitative immunoblotting (Fig. 3A-C). SibA was found in similar amounts at the surface of all strains except the *lmpC* ko, where it was decreased (Fig. 3A). Compared to wt cells, the *lmpA* kd had around 50% less LmpB in the cell lysate and, although not significantly, at the surface (Fig. 3B-C). As expected, no LmpB protein was found in the *lmpB* ko mutant. Interestingly, the *lmpC* ko strain had almost double amounts of LmpB in the cell lysate and about 30% more at its surface (Fig. 3B-C). We conclude that absence of LmpC impairs trafficking of SibA and LmpB to the plasma membrane, though in an opposite manner, without any notable impact on phagocytic uptake (Fig. 2). LmpA is involved in the regulation of the cellular and, to a lower extent, plasma membrane levels of LmpB, which might partly explain the severe defect in mycobacteria uptake of the *lmpA* kd cells (Fig. 2D-F).

The *lmpA* kd mutant has a small adhesion defect

Efficient uptake depends on proper adhesion of the particle to the cell and activation of the actin-dependent engulfment machinery, and many of the most severe phagocytic mutants reported in *D. discoideum* have strong adhesion defects (Cornillon et al., 2008; Cornillon et al., 2000; Fey et al., 2002; Tuxworth et al., 2001). Since our results indicated a strong reduction in mycobacteria uptake, adhesion to *M. smegmatis* was quantitated in all the mutants. Binding to Syto9-labelled bacteria was assayed in cold medium containing sodium azide, conditions that block engulfment. Particle attachment was stabilized by paraformaldehyde (PFA) fixation, and the samples were analysed by flow cytometry. Adhesion to the bacteria was weakly (20%) but significantly reduced in the *lmpA* mutant compared to wt cells (Fig. 3D). Surprisingly, binding of *M. smegmatis* to *lmpB* ko cells was only weakly and insignificantly reduced, indicating that LmpB is not absolutely required for adhesion to *M. smegmatis* under these conditions. We conclude that such small defects likely do not fully explain the strong phagocytic defect of the *lmpA* and *lmpB* mutants.

Knock down of *lmpA* severely impairs random cell motility

If adhesion to the particle is not significantly impaired, the uptake defect is likely caused by the actin-dependent rearrangements to form the cup and/or by the membrane trafficking events associated with phagosome biogenesis. To gain insight into the functionality of the actin cytoskeleton of the *lmp* mutants, the random motility of 20 cells was monitored by live microscopy. The total area of exploration as well as the length of the track were analysed. Both wt and *lmpB* ko cells explored areas of similar size and moved with a speed of 2.00 ± 0.11 µm per minute (Fig. 3E). *lmpC* ko cells migrated slightly faster, with a velocity of 2.50 ± 0.18 µm/min. Knock down of *lmpA*, on the other hand, reduced velocity more than 50% (1.00 ± 0.06 µm/min). This correlates with the area explored by cells within 1 hour: 95% of *lmpA* kd cells visited an area of 175 μm^2, which is about half the area visited by wt cells (383 μm^2) and much more restricted than that visited by *lmpB* and *lmpC* ko cells (937 μm^2) (Sup. Fig. 1B-E insets). In this respect, the phenotypes of the *lmpA* and the *lmpC* mutants diverge, suggesting that actin dynamics might be affected in both strains but in opposite ways, as already observed above for the localisation of surface receptors.

In conclusion, these findings suggest that uptake impairment in the *lmpA* mutant is likely due to actin dynamic defects, while the absence of LmpB, which plays a role restricted to the phagocytic uptake of mycobacteria and *B. subtilis*, does not broadly affect actin cytoskeleton function .

Knock down of *lmpA* impairs cell growth on diverse bacteria

Since LmpA is restricted to the endolysosomal system, we sought to explore whether it might be involved in phagosome maturation, as already reported for mammalian LIMP-2. *D. discoideum* naturally grazes on bacteria and is therefore an excellent system to identify host factors necessary for uptake, but also for killing and digestion. To assess these processes, various assays were performed. First, increasing dilutions of cells were plated on lawns of different bacteria strains (Froquet et al., 2009), and the formation of phagocytic plaques was monitored (Fig. S2A). Formation of a plaque, which is more efficient when cells are deposited in higher numbers, is a global indication that *D. discoideum* can kill, digest and extract nutrients from the respective microbes. Importantly, the bacteria in the lawn are present in a vast excess, which certainly bypasses the uptake defects of the mutant cells. *D. discoideum* does not grow on virulent mycobacteria. However, they can form plaques on a lawn of either non-pathogenic mycobacteria (*M. smegmatis*) or avirulent mutants (*M. marinum* mutant L1D) when they are mixed with the innocuous *K. pneumoniae* in a

1:50-1:500 ratio (Alibaud et al., 2011). Examples of plaque formation are shown in Fig. S2A, and their quantitation is illustrated with a logarithmic scale (Fig. 4A) as well as a colour scale (Fig. S2B). *D. discoideum* wt, *lmpB* ko and *lmpC* ko cells grew equally well on all the bacteria tested, with a growth score of 1000 (see Materials and Methods). Only growth on the Gram-positive bacterium *S. aureus* was slightly decreased for the three strains (Fig. S2A). While *lmpA* kd cells grew relatively well on *Escherichia coli*, *K. pneumoniae* and the clinical isolate *K. pneumoniae* LM21 (Kp21), plaque formation was strongly reduced on Gram-positive bacteria such as *Micrococcus luteus* (40-fold decrease of the growth score) and *S. aureus* (20-fold decrease, Fig. S2B). Interestingly, the growth score of the *lmpA* kd cells on non-pathogenic *M. smegmatis* and avirulent *M. marinum* L1D was also reduced (14-fold and 27-fold, respectively, compared to wt cells). Overall, these data show that knock down of *lmpA* impairs the ability of *D. discoideum* to feed and grow on certain bacterial strains, and that LmpA is likely involved in phagosome maturation.

Another independent and standard assay, the clearing of a suspension of heat-killed bacteria, was used (Peterson et al., 1995). This readout also takes into account several cycles of uptake and digestion. *D. discoideum* was mixed with an excess of *E. coli in phosphate buffer* and the optical density (OD) of the co-culture was measured hourly for 7 hours (Fig. 4B). *D. discoideum* wt and *lmpC* ko cleared bacteria equally well and reached the median clearance at approximately 2 hours, while the *lmpB* ko cleared the same number of bacteria within 5 hours (Fig. 4B). This deficiency might be explained by the weak phagocytosis defect of these cells towards Gram-negative bacteria such as *K. pneumoniae* (Fig. 2B). The *lmpA* kd, on the other hand, showed a 4-fold decreased clearing efficiency, which is in agreement with the results obtained with the plaque assay (Fig. 4A). These data suggest that LmpA is not only involved in particle uptake but has an additional role in killing and/or digestion of bacteria.

D. discoideum LvsB and the adaptor protein complex 3 (AP-3) are both implicated in lysosome biogenesis and postlysosome fusion, processes important for phagosome maturation and for bacterial killing and digestion (Charette and Cosson, 2007; Charette and Cosson, 2008; Charette et al., 2006). Interestingly, the *lvsB* ko and the ko of the AP-3 subunit µ3 formed plaques with a fingerprint comparable to that of the *lmpA* kd cells (see Fig. S2B). These three mutants had specifically low scores for the Gram-positive *M. luteus* and *S. aureus* as well as for *K. pneumoniae*. These findings prompted us to further analyse LmpA's role during bacterial killing, using representative Gram-positive and Gram-negative bacteria (Benghezal et al., 2006). To bypass the uptake defect, bacteria were mixed with a 100–1000-fold excess of *D. discoideum*

cells, ensuring efficient uptake of every bacterium. *K. pneumoniae* or *B. subtilis* were incubated with wt and mutant cells, and samples of the suspension were analysed for colony forming units (cfu) (Benghezal et al., 2006). To assess killing of *M. smegmatis*, we measured the activity of a constitutively expressed firefly luciferase (FFluc) (Andreu et al., 2010). The strong mycobacteria uptake defect of *lmpA* kd and *lmpB* ko cells was bypassed by spinoculating a *D. discoideum* monolayer with *M. smegmatis*. *D. discoideum* wt and *lmpC* ko killed approximately 50% of *K. pneumoniae* within 1 hour, while the *lmpA* and *lmpB* mutants showed a slight but statistically insignificant defect (Fig. 4C). *B. subtilis* was killed by wt and *lmpC* ko cells faster than *K. pneumoniae*, with a median killing at approximately 45 minutes, whereas *lmpA* kd and *lmpB* ko cells killed significantly more slowly this Gram-positive bacterium, with a median killing at 75 minutes (Fig. 4D). None of the mutants showed significant differences in killing *M. smegmatis*, with a median killing at around 6 hours (Fig. 4E).

Overall, these data suggest that the *lmpB* ko has a defect restricted to engulfment of mycobacteria and *B. subtilis*, whereas the *lmpA* mutant might not only be impaired in uptake but also in downstream endolysosomal processes, even though the defects in killing are only mild.

Phagosome acidification and proteolysis are impaired in *lmpA* kd cells

We next investigated the role of the Lmp paralogs during digestion, which directly depends on correct phagosome maturation, lumenal acidification and proteolysis. Fusion of phagosomes with endosomes and lysosomes ensures delivery of the vATPase and subsequent acidification, which is essential for the degradation of the ingested material by hydrolases. Phagosomal pH and proteolytic activity were measured using reporter fluorophores coupled to silica particles (Yates, 2008). The pH-sensitive fluorophore fluorescein isothiocyanate (FITC) was used to monitor the relative kinetics of acidification and reneutralization, while the pH-insensitive dye tetramethylrhodamine isothiocyanate (TRITC) serves as a reference (Dieckmann et al., 2012; Gopaldass et al., 2012; Sattler et al., 2013). The particles were centrifuged onto a cell monolayer, and the change in fluorescence emission was measured with a plate reader. Phagosomes of wt cells acidified instantaneously after phagocytosis, with the lowest FITC/TRITC ratio measured at 30-40 minutes. This values correspond to an approximate pH of 4.5, as previously published (Gopaldass et al., 2012). The kinetics of phagosome acidification in *lmpB* and *lmpC* ko cells was similar to that in wt cells, although the lowest phagosomal pH was reached with a delay of 10 minutes, with

a subsequent delay of about 10-20 minutes for the reneutralization phase(Fig. 5A). Phagosomes of *lmpA* kd cells acidified much more slowly, never reaching a pH as low as in wt cells and were not reneutralized within the time span tested (Fig. 5A).

Because of the possible interference caused by the strong uptake defect of the *lmpA* kd cells (Fig. 2), we validated these measurements of the average population (Fig. 5A) by live microscopy of single cells (Fig. S3A). After addition of FITC/Alexa 594-coupled silica beads, single wt and *lmpA* kd cells were tracked for 3 hours, and the fluorescence emission ratio of 13-23 beads was calculated. Phagosomes of wt cells acidified quickly and reneutralized on average 90 minutes post ingestion (Fig. S3A). The apparently faster and longer acidification phase observed when tracking single beads might be explained by the fact that, in a large cell population, the average of slightly asynchronous acidification and reneutralization steps is measured. Fig. S3B shows snapshots of acidification and reneutralization events at the single cell level. In a wt cell, the phagosome acidified fast with the lowest pH reached at about 17 minutes followed by reneutralization after 29 minutes, and exocytosis after 37.5 min. In contrast, in the *lmpA* kd, the phagosome took longer to acidify and never reached a pH as low as in the wt compartment. Additionally, neither reneutralization nor exocytosis of the bead was observed during the time period monitored. Moreover, the *lmpA* kd moved much more slowly than wt and needed more attempts to take up beads. These findings emphasize again the difficulties in uptake and random cell motility of the *lmpA* mutant.

To monitor phagosomal proteolysis, a similar method was used, with silica beads coupled to the self-quenched reporter DQ Green BSA and the reference dye Alexa 594. Release and dequenching of DQ Green upon BSA degradation by proteolytic enzymes leads to an increase in fluorescence. In phagosomes from wt, *lmpB* ko and *lmpC* ko cells, proteolysis started quickly after uptake, with an initial slope of $3.8x10^{-2}$/min and $2.2x10^{-2}$/min, respectively (Fig. 5B). This rate was decreased 8-fold in *lmpA* kd phagosomes. Also, the *lmpA* kd cells started digestion approximately 30 minutes after phagocytosis, which corresponds to the delay in acidification (Fig. 5A). Overall, these results suggest that the capacity of phagosomes to acidify and proteolyse is strongly reduced in the *lmpA* mutant. Counterintuitively, this defect only weakly impacts the capacity of the *lmpA* mutant to kill "food" bacteria.

The *lmpA* kd has lower levels of lysosomal hydrolases

Deficiency in proteolysis can result from a non-acidic intraphagosomal pH, low enzyme levels and/or altered protein trafficking to the compartment. We first investigated the total cellular content of active lysosomal enzymes by mixing lysates from each cell line with silica beads coupled to DQ Green-BSA and Alexa 594, (Froquet et al., 2008). It should be noted that *D. discoideum* possesses two different sets of lysosomal hydrolases: (i) enzymes such as α-mannosidase, β-glucosidase and cathepsin D, with either mannose-6-phosphomethyldiester (Man-6-P-OCH3) or mannose-6-sulfate (Man-6-SO4 or common antigen 1) modifications, and (ii) enzymes such as cysteine proteases, with an N-acetyl-glucosamine-1-phosphate (GlcNAc-1-P) modification (Souza et al., 1997). Wild type and *lmpC* ko cells had comparable activity of all the enzymes tested. Interestingly, in the *lmpB* ko the activity of N-acetyl-glucosaminidase was elevated by 30%, while the protease activity was around 50% lower. In the *lmpA* kd, however, the overall enzyme activity was reduced. In this context, N-acetyl-mannosidase and N-acetyl-glucosaminidase were both decreased 30-40%, while the activity of proteolytic enzymes was reduced more than 70% (Fig. 6A). Our data suggest that the decreased digestion rates in the *lmpA* mutant phagosome is, at least partly, due to the lower content of total active proteases.

The lower hydrolase activity might result from lower expression levels or from enzyme mistrafficking. To test the latter, we measured the secretion of N-acetyl-mannosidase and N-acetyl-glucosaminidase (Froquet et al., 2008). Cells were incubated with mild shaking for 6 hours in HL5 medium, and supernatants were collected and mixed with the chromogenic enzyme substrates mentioned above. Due to technical reasons, the amount of secreted proteases could not be determined. Intriguingly, while wt and *lmpC* ko cells secreted similar amounts of enzymes, the *lmpB* ko secreted significantly more N-acetyl-glucosaminidase. On the other hand, *lmpA* kd cells secreted around 40% less enzymes (Fig. S3C). Thus, the lower cellular levels of active enzymes in the *lmpA* mutant is not simply due to oversecretion.

Delivery of the cysteine protease CprG is LmpA-dependent

Mammalian LIMP-2 is specifically necessary for the correct trafficking of the enzyme β-glucocerebrosidase (Reczek et al., 2007). It is therefore possible that LmpA has a similar function in *D. discoideum*. To investigate whether trafficking of endosomal/phagosomal proteins is affected in the *lmpA* kd, phagosomes containing latex beads were isolated at various stages of maturation (Gotthardt et al., 2006b), and the levels

of phagosome maturation markers were monitored. Note that immunoblotting is best suited for the relative quantitation of protein amounts between fractions to characterise the overall kinetics, and that the absolute protein levels between different strains has to be analysed separately (Fig. 6B-D). Like in wt cells, the amount of p80 and LmpC increased in the *lmpA* mutant as a function of maturation, while LmpB decreased (Fig. 6B and 1B). In addition, recruitment of the vATPase subunits VatM and VatA, from the subcomplexes V0 and V1, respectively, was comparable in wt and *lmpA* kd cells, suggesting that the acidification defect observed in *lmpA* kd cells is likely not caused by the disassembly of the vATPase. As previously shown (Gopaldass et al., 2012), actin was found at the very early steps of phagosome maturation in wt cells, and decreased drastically 15 minutes after ingestion (Fig. 6C). However, phagosomes from *lmpA* kd cells never lost their associated actin, which even increased two hours post uptake (Fig. 6C). This result corroborates the impairment in actin-related processes of the *lmpA* kd cells (Fig. S1B). In addition, trafficking of the cysteine protease CprG was altered (Fig. 6D). CprG accumulates in wt phagosomes starting around 30 min and is completely removed after 2 hours, while in phagosomes of *lmpA* kd cells, CprG gradually accumulates over time, culminating 3 hours after internalisation. This suggests that the trafficking of CprG in the *lmpA* mutant is perturbed, which might therefore explain to a certain degree the digestion defect. Overall, the data suggest that the reduction in LmpA levels causes a defect in the regulation of actin association with phagosomes and the mistrafficking of at least one lysosomal enzyme, CprG, thereby affecting phagolysosome biogenesis.

Absence of LmpA renders cells more susceptible to infection by pathogenic *M. marinum*

Finally, we wanted to investigate whether the function of LmpA in phagolysosome biogenesis was important for host cell defence against intracellular pathogens such as *M. marinum*. We first wondered whether LmpA was recruited to the *M. marinum*-containing vacuole (MCV). To do so, LmpA-FLAG-expressing cells were infected with *M. marinum*, and the localization of LmpA over the course of the infection was monitored by anti-FLAG immunofluorescence (Fig. 7A). LmpA-FLAG was present at the MCV as early as 3 hours post infection (hpi) and remained associated with the MCV at least for 30 hours (Fig. 7B). In addition, the dynamics of infection with GFP-producing *M. marinum* in wt, *lmpA* kd, *lmpB* ko and *lmpC* ko cells was monitored by flow cytometry. By plotting the side-scatter (SSC) versus the fluorescence (FL1), the population of uninfected cells (1) can be nicely separated from the population of

infected cells (2) and from extracellular bacteria (3) (Fig. S4). In wt, 40-50% of the cells contained bacteria at 0.5 hpi. This proportion of infected cells decreased during the next 2 days of infection (Figs. S4 and 7B), mainly due to the continued replication of *D. discoideum*, with a doubling time of approximately 10 hours. Spinoculation of *lmpA* kd, *lmpB* ko and *lmpC* ko cells resulted in similar initial infection levels, but the respective proportions of infected cells differed markedly at later time points (Fig. 7B). While the percentage of infected *lmpB* ko and *lmpC* ko cells decreased in a manner comparable to the wt strain, the *lmpA* mutant remained highly infected (Fig. S4). Additionally, the normalised total fluorescence during the infection course increased only in *lmpA* mutant cells, reflecting a higher number of intracellular bacteria (Figs. 7C and S4).

Altogether, the results suggest that, even though the absence of both LmpA and LmpB cause a defect in mycobacteria uptake (Fig. 2D-F), only LmpA is a host cell defence factor important during infection with pathogenic mycobacteria.

Discussion

We have characterized *D. discoideum* strains with mutations in the three LIMP2-CD36 homologues, and the phenotypes observed are summarised in Table 1, and schematically represented in Fig 7E, F.

LmpA impacts on phagolysosome biogenesis and digestion

LIMP-2 was suggested to play a role in the biogenesis of endosomes and lysosomes, since its overexpression resulted in large vacuoles with characteristics of early endosomes and late endosomes/lysosomes (Kuronita et al., 2002; Kuronita et al., 2005). On the other hand, lack of LIMP-2 , decreased fusion of phagosomes with lysosomes, affecting susceptibility to bacteria such as *L. monocytogenes* (Carrasco-Marin et al., 2011). In *D. discoideum*, LmpA was proposed to influence fluid transport along the endocytic pathway. FITC-Dextran was retained longer within acidic compartments and the overall exocytosis decreased 3-fold in the *lmpA* kd mutant compared to wt cells (Temesvari et al., 2000). In agreement, our results suggest that LmpA is involved in phagolysosome biogenesis, since two hallmarks of phagosome maturation, acidification and proteolysis, are severely impaired in the *lmpA* mutant (Fig. 5 and 7E). Interestingly, *lvsB* ko and *μ3* ko, two mutants impaired in lysosome biogenesis and exocytosis, (Charette and Cosson, 2007; Charette and Cosson, 2008; Charette et al., 2006; Smith et al., 2010), showed a phagocytic plaque assay fingerprint comparable

to that of *lmpA* kd cells (Fig. S2B). However, contrary to the *lmpA* mutant, the *lvsB* and *μ3* KOs were able to grow on the mycobacteria tested, suggesting that LmpA might have a specific function in resisting these pathogenic bacteria. Most interestingly, despite severe defects in phagosome maturation, the *lmpA* kd is able to grow on *K. pneumoniae* (Fig 4A), i.e. to kill it (Fig. 4C) and digest it. *D. discoideum* kills and digests "food" bacteria, not only via acidic pH and lysosomal hydrolases, but also with ROS, lysozymes and metal ions [for reviews see (Cosson and Lima, 2014; Dunn et al., 2017)]. This suggests that acidification and proteolysis, impaired in the *lmpA* kd mutant, are crucial to kill some but not all types of bacteria, which might require the generation of ROS or the delivery of metal ions such as Zn^{2+} (Soldati and Neyrolles, 2012; Zhang and Soldati, 2016; Zhang et al., 2016).

Phagosome-lysosome fusion might be regulated by LmpA in an actin-dependent manner

Previous reports suggest that LIMP-2 acts downstream of the small GTPase Rab5a to regulate fusion of phagosomes with lysosomes (Carrasco-Marin et al., 2011; Prada-Delgado et al., 2001). However, it is not known how LIMP-2 influences this process. Several actin dependent processes, such as cytokinesis (Karakesisoglou et al., 1999), exocytosis and macropinocytosis (Temesvari et al., 2000) are impaired in the *lmpA* kd mutant. Our experiments confirmed a defect in macropinocytosis, and revealed a decreased uptake of 1 µm latex beads and various bacteria (Fig. 2). In accordance with a proposed role of LmpA in the regulation of the actin cytoskeleton, actin polymerization-dependent processes were affected in the *lmpA* kd, and phagosomes from *lmpA* kd cells never completely lost their associated actin (Fig. 6C), a feature known to inhibit phagosome maturation (Lerm et al., 2006; Liebl and Griffiths, 2009; Meresse et al., 2001). Interestingly, while the *lmpA* mutant had defects in phagocytic uptake and motility, a mutant of the highly evolutionary related LmpC, which also shares cellular localization with LmpA, showed a very different phenotype [i.e. normal uptake and increased random cell motility (Fig. 2 and S1E)]. These divergence might be explained by different expression levels, since LmpC is less abundant than LmpA (Janssen et al., 2001), or by differences in their interactions with other factors, because only LmpA binds to negatively charged phospholipids such as $PI(4,5)P_2$ and PI(4)P (Karakesisoglou et al., 1999; Janssen et al., 2001)). $PI(4,5)P_2$ is usually found at the plasma membrane, but recent reports locate it also to endosomes and lysosomes (Vicinanza et al., 2011).

Trafficking of the lysosomal enzyme CprG is impaired in the *lmpA* kd

Mammalian LIMP-2 is known to bind β-glucocerebrosidase in the ER to ensures its transport to lysosomes (Blanz et al., 2010; Reczek et al., 2007). Absence of LIMP-2 leads to mistargeting of β-glucocerebrosidase to the extracellular space (Reczek et al., 2007), and *Listeria*-containing vacuoles in macrophages from LIMP-2 knock out mice have lower proteolytic activity (Carrasco-Marin et al., 2011).We show that, in *lmpA* kd cells, trafficking of CprG is altered and proteolytic activity is decreased (Fig. 6A and D). However, unlike LIMP-2$^{-/-}$ cells, the *D. discoideum lmpA* mutantdid not oversecrete the enzyme activities tested (Fig. S3C). We speculate that LmpA, similarly to LIMP-2, plays a role in the trafficking of lysosomal enzymes, thereby impacting on digestion. Lysosomal enzymes are synthesized in the ER in an inactive form and subsequent activation by proteolytic processing occurs at acidic pH in endosomes/lysosomes [for a review see (Braulke and Bonifacino, 2009)], a process which is probably affected in the *lmpA* mutant due to its higher lysosomal pH (Fig. 5A).

In *D. discoideum*, two classes of hydrolases are delivered to the phagosome at different times. Whereas enzymes with GlcNAc-1-P modifications such as cysteine proteases are highly enriched at the phagosome 30 min post ingestion of the particle, enzymes with Man-6-SO_4 modifications such as cathepsin D peak 2 hours after phagocytosis (Gotthardt et al., 2002). We show that the overall cellular activity of representatives of the second group of enzymes was only slightly lower in the *lmpA* kd mutant than in wt cells, while the levels of protease activity was strongly decreased in the *lmpA* kd mutant. We interpret this as a sign that LmpA is specifically important for the activity and/or trafficking of one enzyme population.

LmpB might impact on the ingestion of mycobacteria by regulating the actin cytoskeleton

Our results suggest that loss of LmpB specifically inhibits uptake of mycobacteria and *B. subtilis* but not the phagocytosis of other particles (Fig. 2 and 7F). Because absence of LmpB significantly affects uptake but not binding to mycobacteria, this suggests that LmpB is not a direct receptor for mycobacteria. Alternatively, LmpB might be either a co-receptor or a signalling protein necessary to transduce the binding of a mycobacteria and possibly Gram-positive bacteria to its receptor into a triggering of the actin-mediated cup formation. In other words, our findings suggest that LmpB acts as a PRR participating in the recognition of mycobacteria and at least one Gram-positive bacterium and in triggering, directly or indirectly, the actin cytoskeleton remodelling that leads to their ingestion. Moreover, the reduction in *lmpA* expression leads to

a strong, although not significant, decrease in the surface levels of LmpB, which might contribute to the *lmpA* kd mutant defect in mycobacteria and *B. subtilis* uptake. The crosstalk between LmpA, LmpB, LmpC and other bona fide phagocytic receptors, such as those of the Sib family, remains to be investigated.

In conclusion, we show that in *D. discoideum*, LmpA and LmpB act as functional homologues of LIMP-2 and CD36, respectively, corroborating the conserved role of scavenger receptors in professional phagocytes throughout evolution. In addition, we propose LmpA as a host cell defence factor that regulates phagolysosome biogenesis and impacts the fate of pathogenic *M. marinum* infection.

Materials and Methods

Cell culture, cloning and expression procedures

D. discoideum wt (AX2 or DH1-10) were grown axenically at 22°C in HL5 medium (Formedium). The AX2 *lmpA* kd, *lmpB* ko and *lmpC* ko were kindly provided by Dr. M. Schleicher before publication (Janssen et al., 2001; Karakesisoglou et al., 1999). Note that in the *lmpA* kd, LmpA levels are reduced 5 to 10-fold (Karakesisoglou et al., 1999), whereas in the *lmpB* and *lmpC* ko, LmpB and LmpC are absent. *lvsB* and *µ3* were knocked out in the DH1-10 background (Charette and Cosson, 2007; Charette et al., 2006). For epitope tagging, the *lmpA* and *lmpB* coding DNA sequences (CDS) were synthesized with a C-terminal FLAG-tag (Life Technologies). The Tet-Off LmpA-FLAG construct was generated by inserting the synthetic CDS into the pDM309 vector and the Tet-On LmpB-FLAG into the pDM310 (Veltman et al., 2009) between the *Bgl*II and *Spe*I sites. *D. discoideum* was transformed, and cells carrying the FLAG constructs were selected with G418 in the presence of 1 µg/ml of doxycycline to repress expression (pDM309) or without doxycycline (pDM310). To regulate the levels of expression of LmpA-FLAG and LmpB-FLAG in a range similar to that of the endogenous proteins, doxycycline concentrations between 0 and 10 µg/ml were applied for 1 to 2 days.

Bacterial strains and culture

The following bacterial strains were cultured in LB medium at 37°C in shaking, as described previously (Froquet et al., 2009): *K. pneumoniae* strain Kp21 (Favre-Bonte et al., 1999), *P. aeruginosa* avirulent isogenic quorum sensing mutants DP5 (Δ*trpD*) and DP28 (Δ*pchH*) (Alibaud et al., 2008); *E. coli* strain B/r (Gerisch, 1959), *B. subtilis* (Ratner and Newell, 1978), *S. aureus* strain RN6390, and *M. luteus* (Wilczynska

and Fisher, 1994). The unlabelled *M. marinum* M strain (ATCC BAA-535) and *M. smegmatis* were a kind gift of L. Ramakrishnan and G. Griffiths, respectively. These mycobacteria were grown in Middlebrook 7H9 (Difco) supplemented with 10% OADC (Becton Dickinson), 0.4% glycerol and 0.2% Tween 80 (Sigma Aldrich) at 32°C (*M. marinum*) or 37°C (*M. smegmatis*) in shaking as published previously (Arafah et al., 2012; Hagedorn et al., 2009; Hagedorn and Soldati, 2007). *M. marinum* and *M. smegmatis* constitutively producing GFP (Hagedorn and Soldati, 2007) were cultured in presence of 20 μg/ml of kanamycin and *M. marinum* producing mCherry (Carroll et al., 2010) in the presence of 100 μg/ml of hygromycin. *M. smegmatis* producing FFluc was provided by Dr. S. Wiles (Andreu et al., 2010) and cultured in the presence of 50 μg/ml of kanamycin. The *M. marinum* L1D mutant (Ramakrishnan et al., 2000) was grown with 50 μg/ml of apramycin.

Antibodies, immunoblotting and immunofluorescence

Antibodies against LmpA, LmpB and LmpC were obtained from Dr. M. Schleicher (Janssen et al., 2001; Karakesisoglou et al., 1999), CprG from Dr. J. Garin (Journet et al., 1999), actin from Dr. G. Gerisch (Westphal et al., 1997), and VatM (N2) from Dr. R. Allen (Fok et al., 1993). The anti-p80 antibodies were directly-labelled as described in (Ravanel et al., 2001). The monoclonal anti-FLAG-tag antibodies were purchased from Sigma Aldrich. Goat anti-mouse or goat anti-rabbit IgGs coupled to horseradish peroxidase (Biorad) were used as secondary antibodies for immunoblotting, and goat anti-mouse IgGs coupled to Alexa 488 (Thermo Scientific) for immunofluorescence. Western blotting was performed as previously described (Gotthardt et al., 2006b). For immunofluorescence, *D. discoideum* cells were either fixed with PFA/picric acid or with ultra-cold methanol (MeOH) as described previously (Hagedorn et al., 2006). Images were recorded with a Zeiss LSM700 confocal microscope using a 63×1.4 NA or a 100×1.4 NA oil immersion objectives, and processed with the FIJI plugin PureDenoise.

Particle and fluid phase uptake

Assessment of fluorescent particles uptake was performed as previously published (Gotthardt et al., 2006b; Sattler et al., 2013). Data was acquired using a FACScalibur Flow cytometer (BD Biosciences) and analysed with the FlowJo software (TreeStar). The initial rate of uptake was calculated by linear regression of the first 30 minutes of phagocytosis, using standard mathematical softwares such as Microsoft Excel. Fluid

phase uptake was measured as previously published (Froquet et al., 2008), by incubating the cells for 20 minutes with 10 mg/ml Alexa 647-coupled dextran (Molecular Probes). Increase in fluorescence was measured by flow cytometry with a FACSCalibur.

Biotinylation of plasma membrane

The surface of *D. discoideum* cells was coupled in the cold to biotin containing a cleavable cross-linker (EZ link Sulfo – NHS- SS Biotin from Invitrogen). After coupling, excess of crosslinker was quenched with 100 mM glycin in phosphate buffer saline (PBS, pH 6), and cells were washed several times with PBS before solubilisation in RIPA buffer (250 mM Tris pH 7.4, 750 mM NaCl, 5% Triton X-100, 5% sodium deoxycholate and 0.5% SDS). To isolate plasma membrane proteins, cell lysates were incubated with neutravidin agarose beads (Thermo), which had been previously washed twice with RIPA buffer. After overnight incubation at 4°C, the beads were extensively washed with RIPA and 6 M urea. Subsequently, the beads were incubated with a buffer (2% SDS and 1% β -mercaptoethanol in PBS) for protein release. Protein samples were subjected to SDS-PAGE and visualized via immunoblotting.

Adhesion to particles

Adhesion to fluorescent *M. smegmatis* was assessed as described previously (Sattler et al., 2013). Briefly, 4 x 10^8 *M. smegmatis* were labelled with 1 µM of the cell-permeable DNA dye Syto 9 (Invitrogen) for 20 minutes in the dark with shaking. In addition, 2 x 10^6 *D. discoideum* cells in 2 ml of HL5 were synchronized for 2 hours in shaking at 21°C to ensure similar starting conditions. Afterwards, cells were centrifuged for 4 minutes at 500 x *g* and resuspended in phosphate Sorenson buffer (SB: 15 mM KH_2PO_4, 2 mM Na_2HPO_4, pH 6.0) supplemented with 150 mM sorbitol and 5 mM sodium azide. Azide blocks the production of mitochondrial ATP, inducing full contraction of the cortical acto-myosin cytoskeleton, which allows adhesion but neither capture (Flannagan et al., 2010) nor engulfment (Maselli et al., 2002) of particles. Cells were then incubated at 4°C on an ice-cooled metal block covered with a wet paper towel. After extensive washing, bacteria were resuspended in SB-sorbitol-azide and added to the cells at a final particle to cell ratio of 200:1. The suspension was incubated for 15 minutes in the cold. To ensure preservation of the particle-cell attachment, a mild PFA fixation (final concentration 4% PFA) was applied for another 5 minutes. Fluorescence was measured by flow cytometry with a FACSCalibur.

Random cell motility

Random velocity of cells was assessed as described previously (Gebbie et al., 2004). Briefly, 10^4 cells were plated on a glass slide and allowed to settle for 30 minutes in HL5. Movement was monitored every 30 seconds during the course of one hour with a Zeiss Axiovert 100 microscope coupled to a Hamamatsu Orca camera (OpenLab3 software). Cell tracking was performed using the MetaMorph Office software, and the average cell velocity was calculated. Cells that were in contact for long periods of time were not included in the data set, since this interaction modifies their speed. To calculate the total area explored by twenty cells within 1 hour, each cell position was plotted around a common origin. The distribution of these 2400 positions corresponds to a Gaussian distribution. Two times the standard deviation of this Gaussian curve corresponds to the radius of 95% of the area explored by the cells, which was subsequently calculated.

Phagocytic plaque assay

The ability of *D. discoideum* to form plaques on a lawn of bacteria was monitored as described previously (Froquet et al., 2009). Briefly, 50 µl of an overnight bacterial culture was plated on SM-agar (10 g peptone (Oxoid), 1 g yeast extract (Difco), 2.2 g KH_2PO_4, 1 g K_2HPO_4, 1 g $MgSO_4$ x $7H_2O$) with 20% glucose in 1 L of ddH_2O) in wells from a 24-well plate. Serial dilutions of *D. discoideum* (10, 10^2, 10^3 or 10^4 cells) were plated onto the bacterial lawn, and the plates were incubated at 21°C for 4-7 days until plaque formation was visible. A slightly different protocol was used to monitor growth on avirulent *M. marinum* L1D or non-pathogenic *M. smegmatis* (Alibaud et al., 2011). This time, 150-600 µl of a 5 x 10^8 mycobacteria/mL culture was centrifuged and resuspended in 1.2 mL 7H9 containing a 1:10^5 dilution of *K. pneumoniae* that had been grown overnight in LB. 50 µL of this suspension were deposited on wells from a 24-well plate containing 2 mL of 7H10-agar (without OADC). The same dilutions of *D. discoideum* cells were added as described above and plaque formation was monitored after 7-11 days at 25°C. To quantify cell growth on bacteria, a logarithmic growth score was assigned as follows: plaque formation up to a dilution of 10 cells received a score of 1000; when cells were not able to grow at lower dilutions, they obtained the corresponding lower scores of 100, 10 and 1.

Clearing of* heat-killed *E. coli

Clearing of heat-killed *E. coli* was performed as described previously (Peterson et al., 1995). Briefly, an *E. coli* B/r culture was grown to an OD_{600} of 0.4 and subsequently autoclaved. Heat-killed bacteria were then washed with 17 mM SB. 10^7 wt or mutant cells were resuspended in 10 mL of the bacterial suspension, and they were incubated in shaking at 22°C. As readout for clearance, the OD_{600} was measured hourly during 7 hours.

Killing assay

Killing of *K. pneumoniae* or *B. subtilis* was monitored as described previously (Benghezal et al., 2006). Briefly, 10^6 *D. discoideum* cells were mixed in 500 µl of SB with either 5 x 10^3 *K. pneumoniae* or 5 x 10^4 *B. subtilis* from an overnight culture (grown in LB at 170 rpm and 37°C). After either 0, 1, 2 or 4 hours (*K. pneumoniae*) or 0, 15, 30, 45, 60, 90 or 120 minutes (*B. subtilis*) of incubation, 10 µl aliquots were lysed in the cold in 40% sucrose and 0.5% saponin, and lysates were plated on LB-agar plates for CFU counting. To monitor killing of *M. smegmatis*, a different protocol was established. In this case, bioluminescent *M. smegmatis* expressing FFluc (Andreu et al., 2010) were grown at 25°C in shaking until a density of 5 x 10^8 bacteria/mL was reached. Then, 5 x 10^6 bacteria were washed and resuspended in 500 µl of HL5, and they were passaged at least 4 times through a blunt 25-gauge needle to disrupt bacterial clumps. Bacteria were added at a MOI of 10 and centrifuged twice onto a *D. discoideum* cell layer at 500 x *g* for 10 minutes. Afterwards, cells were allowed to phagocytose for another 10 minutes at 25°C in static. Extracellular bacteria were then washed off, and cells were subsequently detached and resuspended in 5 mL of HL5. The suspension was incubated in silanised beakers (with Repel-Silane ES, Amersham Biosciences) at 32°C and 150 rpm. 300 µl aliquots of the suspension were pelleted in triplicates at 0, 1, 3, 6 or 24 hours, lysed with 100 µl 0.2% Triton-X-100 in PBS, and transferred to white opaque 96-well plates (Nunc). After 10 minutes of incubation, the background luminescence was measured using a bioluminescence plate reader (Synergy Mx). To detect live bacteria, luciferin (Gold Biotechnology) was added at a final concentration of 150 µg/mL, and luminescence was measured.

Acidification and proteolysis

The kinetics of acidification and proteolytic activity inside phagosomes were monitored as described previously (Gopaldass et al., 2012; Sattler et al., 2013). In order to precisely monitor the relative kinetics of acidification and reneutralization, phagosomal pH was monitored using the reporter fluorophore FITC (Molecular Probes) (pKa 6.4) coupled to 3 µm silica particles (Kisker Biotech) (Dieckmann et al., 2012; Gopaldass et al., 2012; Sattler et al., 2013; Yates, 2008). Beads were also coated with the pH-insensitive TRITC (Molecular Probes) as a reference dye. After centrifugation of the silica particles at a ratio of 1:2 onto a *D. discoideum* cell monolayer in clear-bottom black-wall 96-well dishes (Perkin Elmer), uningested beads were removed by thorough washing with low fluorescence medium (LoFlo, Formedium). Subsequently, the ratio of fluorescence emission (520 nm / 620 nm) was measured every minute over a period of 150 minutes with a fluorescence plate reader (Synergy Mx, Biotek). To monitor acidification at the single cell level, cells were plated on 35-mm ibidi dishes (ibidi GmbH, Germany, ref# 80136), and 30 minutes before imaging HL5 was replaced by LoFlo. 10 µl of FITC/TRITC-coupled silica beads (stock concentration, 1.25 x 10^{10} beads/mL) were added just before imaging. Cells were then overlaid with a thin sheet of 1% agar in LoFlo, as described previously (Clarke et al., 2010). Movies were recorded with a Leica AF6000LX widefield microscope using a 63x glycerol objective. Images were taken every 30 seconds during 3-4 hours. Tracking of bead-containing phagosomes and calculations of their emitted fluorescence ratios were done with the help of the Imaris software (Bitplane). Proteolysis was measured using beads coupled to the reference stain Alexa 594 (Molecular Probes) and the reporter DQ Green-BSA (Molecular Probes) at a self-quenching concentration. Upon proteolysis of BSA, DQ Green is released and dequenched, which causes an increase in fluorescence. The initial rate of proteolysis was calculated by fitting a line with linear regression throughout the first 30 minutes of digestion, using standard mathematical software such as Microsoft Excel.

Measurement of lysosomal enzyme content and secretion

To measure the cellular content and secretion of the lysosomal enzymes N-acetyl-glucosaminidase or N-acetyl-mannosidase, a previously described protocol was used (Froquet et al., 2008). 10^6 cells were incubated in fresh HL5 for 6 hours at 21°C with mild shaking. After centrifugation, the supernatant was recovered, and the pellet was lysed with 0.1% Triton-X-100 in HL5. 50 µl of either supernatant or lysed pellet were mixed with 50 µl of a chromogenic enzyme substrate (10 mM substrate in 5 mM NaOAc, pH 5.2) and incubated at 37°C for 1 hour. The reaction was stopped by adding 500 mM Na_2CO_3 and the OD_{405} was measured with an ELISA microplate reader. The substrates p-nitrophenyl N-acetyl-D-glucosaminide, and p-nitrophenyl-D-mannopyranoside (Sigma) were dissolved in dimethylformamide at a concentration of 250 mM and stored at -20°C. Cellular protease content was measured with a newly established protocol. 4 x 10^6 cells were resuspended in 150 mM K-acetate buffer (pH 4) and lysed by repeated cycles of freezing in liquid nitrogen and thawing. The lysate and 8 µl of silica beads coupled to the self-quenching reporter DQ Green-BSA and the reference dye Alexa 594 (stock concentration 1.25 x 10^{10} beads/mL) were transferred into wells of a clear-bottom black-wall 96-well dishes (Perkin Elmer). Digestion of BSA only occurs at acidic pH, which is crucial for the activity of proteolytic enzymes. Increase in fluorescence was measured with the Synergy Mx (Biotek) fluorescence microplate reader.

Phagosome isolation

Phagosomes containing latex beads were purified via flotation on sucrose gradients and processed exactly as described previously (Dieckmann et al., 2008; Gotthardt et al., 2006b).

Infection with pathogenic mycobacteria

Infection of *D. discoideum* with pathogenic mycobacteria was performed as described previously (Cardenal-Munoz et al., 2017). Briefly, mycobacteria were grown to a density of 5 x 10^8 bacteria/mL, washed with HL5 and passaged through a blunt 25-gauge needle for declumping. 5 x 10^7 *D. discoideum* cells were plated on a 10 cm Petri dish and let attach for 20 minutes at 25°C. Bacteria were added at a MOI of 10, and infection was synchronized by centrifuging twice for 10 minutes wt 500 x *g*. To ensure an efficient phagocytosis, cells were left in static for another 15 minutes at 25°C, before extracellular bacteria were washed off with HL5. Cells were resuspended in 37.5 mL of HL5 containing 5 mg/mL of streptomycin to inhibit growth of

putative remaining extracellular bacteria. The suspension was incubated for up to 2 days at 25°C in shaking at 150 rpm. To analyse the kinetics of the infection by flow cytometry, cells were infected with GFP-producing *M. marinum*, and the increase in fluorescence was monitored as described previously (Hagedorn and Soldati, 2007). To directly assess the number of live and fit bacteria, cells were infected with *M. marinum* expressing the pMV306-lux plasmid (Andreu et al., 2010; Arafah et al., 2012), and luminescence was measured with the plate reader Synergy Mx (Biotek). To assess the localization of LmpA during infection, non-labelled or mCherry-producing *M, marinum* were used to infect *lmpA* kd cells expressing LmpA-FLAG and fixed with PFA/picric acid at 3, 21 and 29 hpi.

Acknowledgements

We thank Dr. Régis Dieckmann, Dr Sonia Arafah and Stéphanie Hausherr for their help with preliminary experiments. We also thank Dr. Wanessa de Lima and Dr. Emmanuelle Alborini for their help with the phagocytic plaque and killing assays. We are grateful to Dr. Michael Schleicher for sharing strains, antibodies and information prior to publication. We thank Dr. Ulrich Schaible and especially Dr. Elena Cardenal-Muñoz for careful reading of the manuscript and thoughtful suggestions. This work was supported by multiple grants from the Swiss National Science Foundation.

References

Alibaud, L., Kohler, T., Coudray, A., Prigent-Combaret, C., Bergeret, E., Perrin, J., Benghezal, M., Reimmann, C., Gauthier, Y., van Delden, C. et al. (2008). Pseudomonas aeruginosa virulence genes identified in a Dictyostelium host model. *Cell Microbiol* **10**, 729-40.

Alibaud, L., Rombouts, Y., Trivelli, X., Burguiere, A., Cirillo, S. L., Cirillo, J. D., Dubremetz, J. F., Guerardel, Y., Lutfalla, G. and Kremer, L. (2011). A Mycobacterium marinum TesA mutant defective for major cell wall-associated lipids is highly attenuated in Dictyostelium discoideum and zebrafish embryos. *Mol Microbiol* **80**, 919-34.

Andreu, N., Zelmer, A., Fletcher, T., Elkington, P. T., Ward, T. H., Ripoll, J., Parish, T., Bancroft, G. J., Schaible, U., Robertson, B. D. et al. (2010). Optimisation of bioluminescent reporters for use with mycobacteria. *PLoS One* **5**, e10777.

Arafah, S., K., K., M., H., N., A., S., W., B., R. and T., S. (2012). Infection with mycobacteria.

Arafah, S., Kicka, S., Trofimov, V., Hagedorn, M., Andreu, N., Wiles, S., Robertson, B. and Soldati, T. (2013). Setting up and monitoring an infection of Dictyostelium discoideum with mycobacteria. *Methods Mol Biol* **983**, 403-17.

Areschoug, T. and Gordon, S. (2009). Scavenger receptors: role in innate immunity and microbial pathogenesis. *Cell Microbiol* **11**, 1160-9.

Aubry, L., Klein, G., Martiel, J. L. and Satre, M. (1993). Kinetics of endosomal pH evolution in Dictyostelium discoideum amoebae. Study by fluorescence spectroscopy. *J Cell Sci* **105 (Pt 3)**, 861-6.

Augenstreich, J., Arbues, A., Simeone, R., Haanappel, E., Wegener, A., Sayes, F., Le Chevalier, F., Chalut, C., Malaga, W., Guilhot, C. et al. (2017). ESX-1 and phthiocerol dimycocerosates of Mycobacterium tuberculosis act in concert to cause phagosomal rupture and host cell apoptosis. *Cell Microbiol* **19**.

Baranova, I. N., Bocharov, A. V., Vishnyakova, T. G., Kurlander, R., Chen, Z., Fu, D., Arias, I. M., Csako, G., Patterson, A. P. and Eggerman, T. L. (2010). CD36 is a novel serum amyloid A (SAA) receptor mediating SAA binding and SAA-induced signaling in human and rodent cells. *J Biol Chem* **285**, 8492-506.

Baranova, I. N., Kurlander, R., Bocharov, A. V., Vishnyakova, T. G., Chen, Z., Remaley, A. T., Csako, G., Patterson, A. P. and Eggerman, T. L. (2008). Role of human CD36 in bacterial recognition, phagocytosis, and pathogen-induced JNK-mediated signaling. *J Immunol* **181**, 7147-56.

Barisch, C., Lopez-Jimenez, A. T. and Soldati, T. (2015). Live imaging of Mycobacterium marinum infection in Dictyostelium discoideum. *Methods Mol Biol* **1285**, 369-85.

Benghezal, M., Fauvarque, M. O., Tournebize, R., Froquet, R., Marchetti, A., Bergeret, E., Lardy, B., Klein, G., Sansonetti, P., Charette, S. J. et al. (2006). Specific host genes required for the killing of Klebsiella bacteria by phagocytes. *Cell Microbiol* **8**, 139-48.

Blanz, J., Groth, J., Zachos, C., Wehling, C., Saftig, P. and Schwake, M. (2010). Disease-causing mutations within the lysosomal integral membrane protein type 2 (LIMP-2) reveal the nature of binding to its ligand beta-glucocerebrosidase. *Hum Mol Genet* **19**, 563-72.

Blanz, J., Zunke, F., Markmann, S., Damme, M., Braulke, T., Saftig, P. and Schwake, M. (2015). Mannose 6-phosphate-independent Lysosomal Sorting of LIMP-2. *Traffic* **16**, 1127-36.

Boulais, J., Trost, M., Landry, C. R., Dieckmann, R., Levy, E. D., Soldati, T., Michnick, S. W., Thibault, P. and Desjardins, M. (2010). Molecular characterization of the evolution of phagosomes. *Mol Syst Biol* **6**, 423.

Bozzaro, S., Bucci, C. and Steinert, M. (2008). Phagocytosis and host-pathogen interactions in Dictyostelium with a look at macrophages. *Int Rev Cell Mol Biol* **271**, 253-300.

Braulke, T. and Bonifacino, J. S. (2009). Sorting of lysosomal proteins. *Biochim Biophys Acta* **1793**, 605-14.

Buckley, C. M., Gopaldass, N., Bosmani, C., Johnston, S. A., Soldati, T., Insall, R. H. and King, J. S. (2016). WASH drives early recycling from macropinosomes and phagosomes to maintain surface phagocytic receptors. *Proc Natl Acad Sci U S A* **113**, E5906-E5915.

Cardenal-Munoz, E., Barisch, C., Lefrancois, L. H., Lopez-Jimenez, A. T. and Soldati, T. (2017). When Dicty Met Myco, a (Not So) Romantic Story about One Amoeba and Its Intracellular Pathogen. *Front Cell Infect Microbiol* **7**, 529.

Carrasco-Marin, E., Fernandez-Prieto, L., Rodriguez-Del Rio, E., Madrazo-Toca, F., Reinheckel, T., Saftig, P. and Alvarez-Dominguez, C. (2011). LIMP-2 links late phagosomal trafficking with the onset of the innate immune response to Listeria monocytogenes: a role in macrophage activation. *J Biol Chem* **286**, 3332-41.

Carroll, P., Schreuder, L. J., Muwanguzi-Karugaba, J., Wiles, S., Robertson, B. D., Ripoll, J., Ward, T. H., Bancroft, G. J., Schaible, U. E. and Parish, T. (2010). Sensitive detection of gene expression in mycobacteria under replicating and non-replicating conditions using optimized far-red reporters. *PLoS One* **5**, e9823.

Charette, S. J. and Cosson, P. (2007). A LYST/beige homolog is involved in biogenesis of Dictyostelium secretory lysosomes. *J Cell Sci* **120**, 2338-43.

Charette, S. J. and Cosson, P. (2008). Altered composition and secretion of lysosome-derived compartments in Dictyostelium AP-3 mutant cells. *Traffic* **9**, 588-96.

Charette, S. J., Mercanti, V., Letourneur, F., Bennett, N. and Cosson, P. (2006). A role for adaptor protein-3 complex in the organization of the endocytic pathway in Dictyostelium. *Traffic* **7**, 1528-38.

Chia, C. P. (1996). A 130-kDa plasma membrane glycoprotein involved in Dictyostelium phagocytosis. *Exp Cell Res* **227**, 182-9.

Clarke, M., Kohler, J., Arana, Q., Liu, T., Heuser, J. and Gerisch, G. (2002). Dynamics of the vacuolar H(+)-ATPase in the contractile vacuole complex and the endosomal pathway of Dictyostelium cells. *J Cell Sci* **115**, 2893-905.

Clarke, M., Maddera, L., Engel, U. and Gerisch, G. (2010). Retrieval of the vacuolar H-ATPase from phagosomes revealed by live cell imaging. *PLoS One* **5**, e8585.

Cornillon, S., Froquet, R. and Cosson, P. (2008). Involvement of Sib proteins in the regulation of cellular adhesion in Dictyostelium discoideum. *Eukaryot Cell* **7**, 1600-5.

Cornillon, S., Gebbie, L., Benghezal, M., Nair, P., Keller, S., Wehrle-Haller, B., Charette, S. J., Bruckert, F., Letourneur, F. and Cosson, P. (2006). An adhesion molecule in free-living Dictyostelium amoebae with integrin beta features. *EMBO Rep* **7**, 617-21.

Cornillon, S., Pech, E., Benghezal, M., Ravanel, K., Gaynor, E., Letourneur, F., Bruckert, F. and Cosson, P. (2000). Phg1p is a nine-transmembrane protein superfamily member involved in dictyostelium adhesion and phagocytosis. *J Biol Chem* **275**, 34287-92.

Cosson, P. and Lima, W. C. (2014). Intracellular killing of bacteria: is Dictyostelium a model macrophage or an alien? *Cell Microbiol* **16**, 816-23.

Cosson, P. and Soldati, T. (2008). Eat, kill or die: when amoeba meets bacteria. *Curr Opin Microbiol* **11**, 271-6.

Court, N., Vasseur, V., Vacher, R., Fremond, C., Shebzukhov, Y., Yeremeev, V. V., Maillet, I., Nedospasov, S. A., Gordon, S., Fallon, P. G. et al. (2010). Partial redundancy of the pattern recognition receptors, scavenger receptors, and C-type lectins for the long-term control of Mycobacterium tuberculosis infection. *J Immunol* **184**, 7057-70.

Dieckmann, R., Gopaldass, N., Escalera, C. and Soldati, T. (2008). Monitoring time-dependent maturation changes in purified phagosomes from Dictyostelium discoideum. *Methods Mol Biol* **445**, 327-37.

Dieckmann, R., Gueho, A., Monroy, R., Ruppert, T., Bloomfield, G. and Soldati, T. (2012). The balance in the delivery of ER components and the vacuolar proton pump to the phagosome depends on myosin IK in Dictyostelium. *Mol Cell Proteomics* **11**, 886-900.

Dunn, J. D., Bosmani, C., Barisch, C., Raykov, L., Lefrancois, L. H., Cardenal-Munoz, E., Lopez-Jimenez, A. T. and Soldati, T. (2017). Eat Prey, Live: Dictyostelium discoideum As a Model for Cell-Autonomous Defenses. *Front Immunol* **8**, 1906.

Eichinger, L., Pachebat, J. A., Glockner, G., Rajandream, M. A., Sucgang, R., Berriman, M., Song, J., Olsen, R., Szafranski, K., Xu, Q. et al. (2005). The genome of the social amoeba Dictyostelium discoideum. *Nature* **435**, 43-57.

Favre-Bonte, S., Joly, B. and Forestier, C. (1999). Consequences of reduction of Klebsiella pneumoniae capsule expression on interactions of this bacterium with epithelial cells. *Infect Immun* **67**, 554-61.

Fey, P., Stephens, S., Titus, M. A. and Chisholm, R. L. (2002). SadA, a novel adhesion receptor in Dictyostelium. *J Cell Biol* **159**, 1109-19.

Flannagan, R. S., Harrison, R. E., Yip, C. M., Jaqaman, K. and Grinstein, S. (2010). Dynamic macrophage "probing" is required for the efficient capture of phagocytic targets. *J Cell Biol* **191**, 1205-18.

Fok, A. K., Clarke, M., Ma, L. and Allen, R. D. (1993). Vacuolar H(+)-ATPase of Dictyostelium discoideum. A monoclonal antibody study. *J Cell Sci* **106 (Pt 4)**, 1103-13.

Froquet, R., Cherix, N., Birke, R., Benghezal, M., Cameroni, E., Letourneur, F., Mosch, H. U., De Virgilio, C. and Cosson, P. (2008). Control of cellular physiology by TM9 proteins in yeast and Dictyostelium. *J Biol Chem* **283**, 6764-72.

Froquet, R., le Coadic, M., Perrin, J., Cherix, N., Cornillon, S. and Cosson, P. (2012). TM9/Phg1 and SadA proteins control surface expression and stability of SibA adhesion molecules in Dictyostelium. *Mol Biol Cell* **23**, 679-86.

Froquet, R., Lelong, E., Marchetti, A. and Cosson, P. (2009). Dictyostelium discoideum: a model host to measure bacterial virulence. *Nat Protoc* **4**, 25-30.

Fuchs, B. B. and Mylonakis, E. (2006). Using non-mammalian hosts to study fungal virulence and host defense. *Curr Opin Microbiol* **9**, 346-51.

Gebbie, L., Benghezal, M., Cornillon, S., Froquet, R., Cherix, N., Malbouyres, M., Lefkir, Y., Grangeasse, C., Fache, S., Dalous, J. et al. (2004). Phg2, a kinase involved in adhesion and focal site modeling in Dictyostelium. *Mol Biol Cell* **15**, 3915-25.

Gerisch, G. (1959). Ein Submerskulturverfahren fur entwicklungsphysiologische Untersuchungen an *Dictyostelium discoideum*. *Naturwissenschaften* **46**, 654–656.

Gonzalez, A., Valeiras, M., Sidransky, E. and Tayebi, N. (2014). Lysosomal integral membrane protein-2: a new player in lysosome-related pathology. *Mol Genet Metab* **111**, 84-91.

Gopaldass, N., Patel, D., Kratzke, R., Dieckmann, R., Hausherr, S., Hagedorn, M., Monroy, R., Kruger, J., Neuhaus, E. M., Hoffmann, E. et al. (2012). Dynamin A, Myosin IB and Abp1 couple phagosome maturation to F-actin binding. *Traffic* **13**, 120-30.

Gotthardt, D., Blancheteau, V., Bosserhoff, A., Ruppert, T., Delorenzi, M. and Soldati, T. (2006a). Proteomics fingerprinting of phagosome maturation and evidence for the role of a Galpha during uptake. *Mol Cell Proteomics* **5**, 2228-43.

Gotthardt, D., Dieckmann, R., Blancheteau, V., Kistler, C., Reichardt, F. and Soldati, T. (2006b). Preparation of intact, highly purified phagosomes from Dictyostelium. *Methods Mol Biol* **346**, 439-48.

Gotthardt, D., Warnatz, H. J., Henschel, O., Bruckert, F., Schleicher, M. and Soldati, T. (2002). High-resolution dissection of phagosome maturation reveals distinct membrane trafficking phases. *Mol Biol Cell* **13**, 3508-20.

Haas, A. (2007). The phagosome: compartment with a license to kill. *Traffic* **8**, 311-30.

Hagedorn, M., Neuhaus, E. M. and Soldati, T. (2006). Optimized fixation and immunofluorescence staining methods for Dictyostelium cells. *Methods Mol Biol* **346**, 327-38.

Hagedorn, M., Rohde, K. H., Russell, D. G. and Soldati, T. (2009). Infection by tubercular mycobacteria is spread by nonlytic ejection from their amoeba hosts. *Science* **323**, 1729-33.

Hagedorn, M. and Soldati, T. (2007). Flotillin and RacH modulate the intracellular immunity of Dictyostelium to Mycobacterium marinum infection. *Cell Microbiol* **9**, 2716-33.

Hagedorn, M. and Soldati, T. (2009). Mycobacterium marinum In *Intracellular Niches of Microbes: A Pathogens Guide Through the Host Cell*, (eds **U. E. Schaible** and **A. Haas**), pp. 455-467: John Wiley & Sons, Ltd.

Hagele, S., Kohler, R., Merkert, H., Schleicher, M., Hacker, J. and Steinert, M. (2000). Dictyostelium discoideum: a new host model system for intracellular pathogens of the genus Legionella. *Cell Microbiol* **2**, 165-71.

Harris, T. J., Awrey, D. E., Cox, B. J., Ravandi, A., Tsang, A. and Siu, C. H. (2001a). Involvement of a triton-insoluble floating fraction in Dictyostelium cell-cell adhesion. *J Biol Chem* **276**, 18640-8.

Harris, T. J., Ravandi, A. and Siu, C. H. (2001b). Assembly of glycoprotein-80 adhesion complexes in Dictyostelium. Receptor compartmentalization and oligomerization in membrane rafts. *J Biol Chem* **276**, 48764-74.

Hoebe, K., Georgel, P., Rutschmann, S., Du, X., Mudd, S., Crozat, K., Sovath, S., Shamel, L., Hartung, T., Zahringer, U. et al. (2005). CD36 is a sensor of diacylglycerides. *Nature* **433**, 523-7.

Janssen, K. P., Rost, R., Eichinger, L. and Schleicher, M. (2001). Characterization of CD36/LIMPII homologues in Dictyostelium discoideum. *J Biol Chem* **276**, 38899-910.

Jia, K., Thomas, C., Akbar, M., Sun, Q., Adams-Huet, B., Gilpin, C. and Levine, B. (2009). Autophagy genes protect against Salmonella typhimurium infection and mediate insulin signaling-regulated pathogen resistance. *Proc Natl Acad Sci U S A* **106**, 14564-9.

Journet, A., Chapel, A., Jehan, S., Adessi, C., Freeze, H., Klein, G. and Garin, J. (1999). Characterization of Dictyostelium discoideum cathepsin D. *J Cell Sci* **112 (Pt 21)**, 3833-43.

Karakesisoglou, I., Janssen, K. P., Eichinger, L., Noegel, A. A. and Schleicher, M. (1999). Identification of a suppressor of the Dictyostelium profilin-minus phenotype as a CD36/LIMP-II homologue. *J Cell Biol* **145**, 167-81.

Koller, B., Schramm, C., Siebert, S., Triebel, J., Deland, E., Pfefferkorn, A. M., Rickerts, V. and Thewes, S. (2016). Dictyostelium discoideum as a Novel Host System to Study the Interaction between Phagocytes and Yeasts. *Front Microbiol* **7**, 1665.

Kuronita, T., Eskelinen, E. L., Fujita, H., Saftig, P., Himeno, M. and Tanaka, Y. (2002). A role for the lysosomal membrane protein LGP85 in the biogenesis and maintenance of endosomal and lysosomal morphology. *J Cell Sci* **115**, 4117-31.

Kuronita, T., Hatano, T., Furuyama, A., Hirota, Y., Masuyama, N., Saftig, P., Himeno, M., Fujita, H. and Tanaka, Y. (2005). The NH(2)-terminal transmembrane and lumenal domains of LGP85 are needed for the formation of enlarged endosomes/lysosomes. *Traffic* **6**, 895-906.

Lelong, E., Marchetti, A., Gueho, A., Lima, W. C., Sattler, N., Molmeret, M., Hagedorn, M., Soldati, T. and Cosson, P. (2011). Role of magnesium and a phagosomal P-type ATPase in intracellular bacterial killing. *Cell Microbiol* **13**, 246-58.

Lerm, M., Holm, A., Seiron, A., Sarndahl, E., Magnusson, K. E. and Rasmusson, B. (2006). Leishmania donovani requires functional Cdc42 and Rac1 to prevent phagosomal maturation. *Infect Immun* **74**, 2613-8.

Liebl, D. and Griffiths, G. (2009). Transient assembly of F-actin by phagosomes delays phagosome fusion with lysosomes in cargo-overloaded macrophages. *J Cell Sci* **122**, 2935-45.

Maniak, M. (2003). Fusion and fission events in the endocytic pathway of Dictyostelium. *Traffic* **4**, 1-5.

Maselli, A., Laevsky, G. and Knecht, D. A. (2002). Kinetics of binding, uptake and degradation of live fluorescent (DsRed) bacteria by Dictyostelium discoideum. *Microbiology* **148**, 413-20.

Means, T. K., Mylonakis, E., Tampakakis, E., Colvin, R. A., Seung, E., Puckett, L., Tai, M. F., Stewart, C. R., Pukkila-Worley, R., Hickman, S. E. et al. (2009). Evolutionarily conserved recognition and innate immunity to fungal pathogens by the scavenger receptors SCARF1 and CD36. *J Exp Med* **206**, 637-53.

Meresse, S., Unsworth, K. E., Habermann, A., Griffiths, G., Fang, F., Martinez-Lorenzo, M. J., Waterman, S. R., Gorvel, J. P. and Holden, D. W. (2001). Remodelling of the actin cytoskeleton is essential for replication of intravacuolar Salmonella. *Cell Microbiol* **3**, 567-77.

Miyata, S. T., Kitaoka, M., Brooks, T. M., McAuley, S. B. and Pukatzki, S. (2011). Vibrio cholerae requires the type VI secretion system virulence factor VasX to kill Dictyostelium discoideum. *Infect Immun* **79**, 2941-9.

Neculai, D., Schwake, M., Ravichandran, M., Zunke, F., Collins, R. F., Peters, J., Neculai, M., Plumb, J., Loppnau, P., Pizarro, J. C. et al. (2013). Structure of LIMP-2 provides functional insights with implications for SR-BI and CD36. *Nature* **504**, 172-6.

Pan, M., Xu, X., Chen, Y. and Jin, T. (2016). Identification of a Chemoattractant G-Protein-Coupled Receptor for Folic Acid that Controls Both Chemotaxis and Phagocytosis. *Dev Cell* **36**, 428-39.

Peterson, M. D., Novak, K. D., Reedy, M. C., Ruman, J. I. and Titus, M. A. (1995). Molecular genetic analysis of myoC, a Dictyostelium myosin I. *J Cell Sci* **108 (Pt 3)**, 1093-103.

Philips, J. A., Rubin, E. J. and Perrimon, N. (2005). Drosophila RNAi screen reveals CD36 family member required for mycobacterial infection. *Science* **309**, 1251-3.

Prada-Delgado, A., Carrasco-Marin, E., Bokoch, G. M. and Alvarez-Dominguez, C. (2001). Interferon-gamma listericidal action is mediated by novel Rab5a functions at the phagosomal environment. *J Biol Chem* **276**, 19059-65.

Ramakrishnan, L., Federspiel, N. A. and Falkow, S. (2000). Granuloma-specific expression of Mycobacterium virulence proteins from the glycine-rich PE-PGRS family. *Science* **288**, 1436-9.

Ratner, D. I. and Newell, P. C. (1978). Linkage analysis in Dictyostelium discoideum using multiply marked tester strains: establishment of linkage group VII and the reassessment of earlier linkage data. *J Gen Microbiol* **109**, 225-36.

Ravanel, K., de Chassey, B., Cornillon, S., Benghezal, M., Zulianello, L., Gebbie, L., Letourneur, F. and Cosson, P. (2001). Membrane sorting in the endocytic and phagocytic pathway of Dictyostelium discoideum. *Eur J Cell Biol* **80**, 754-64.

Reczek, D., Schwake, M., Schroder, J., Hughes, H., Blanz, J., Jin, X., Brondyk, W., Van Patten, S., Edmunds, T. and Saftig, P. (2007). LIMP-2 is a receptor for lysosomal mannose-6-phosphate-independent targeting of beta-glucocerebrosidase. *Cell* **131**, 770-83.

Sattler, N., Monroy, R. and Soldati, T. (2013). Quantitative analysis of phagocytosis and phagosome maturation. *Methods Mol Biol* **983**, 383-402.

Schafer, G., Guler, R., Murray, G., Brombacher, F. and Brown, G. D. (2009). The role of scavenger receptor B1 in infection with Mycobacterium tuberculosis in a murine model. *PLoS One* **4**, e8448.

Silverstein, R. L. and Febbraio, M. (2009). CD36, a scavenger receptor involved in immunity, metabolism, angiogenesis, and behavior. *Sci Signal* **2**, re3.

Simeone, R., Bobard, A., Lippmann, J., Bitter, W., Majlessi, L., Brosch, R. and Enninga, J. (2011). Phagosomal rupture by Mycobacterium tuberculosis results in toxicity and host cell death. *PLoS Pathog* **8**, e1002507.

Simeone, R., Sayes, F., Song, O., Groschel, M. I., Brodin, P., Brosch, R. and Majlessi, L. (2015). Cytosolic access of Mycobacterium tuberculosis: critical impact of phagosomal acidification control and demonstration of occurrence in vivo. *PLoS Pathog* **11**, e1004650.

Smith, E. W., Lima, W. C., Charette, S. J. and Cosson, P. (2010). Effect of starvation on the endocytic pathway in Dictyostelium cells. *Eukaryot Cell* **9**, 387-92.

Soldati, T. and Neyrolles, O. (2012). Mycobacteria and the Intraphagosomal Environment: Take It With a Pinch of Salt(s)! *Traffic*.

Solomon, J. M., Leung, G. S. and Isberg, R. R. (2003). Intracellular replication of Mycobacterium marinum within Dictyostelium discoideum: efficient replication in the absence of host coronin. *Infect Immun* **71**, 3578-86.

Souza, G. M., Mehta, D. P., Lammertz, M., Rodriguez-Paris, J., Wu, R., Cardelli, J. A. and Freeze, H. H. (1997). Dictyostelium lysosomal proteins with different sugar modifications sort to functionally distinct compartments. *J Cell Sci* **110 (Pt 18)**, 2239-48.

Steinert, M. and Heuner, K. (2005). Dictyostelium as host model for pathogenesis. *Cell Microbiol* **7**, 307-14.

Stuart, L. M., Deng, J., Silver, J. M., Takahashi, K., Tseng, A. A., Hennessy, E. J., Ezekowitz, R. A. and Moore, K. J. (2005). Response to Staphylococcus aureus requires CD36-mediated phagocytosis triggered by the COOH-terminal cytoplasmic domain. *J Cell Biol* **170**, 477-85.

Sturgill-Koszycki, S., Schlesinger, P. H., Chakraborty, P., Haddix, P. L., Collins, H. L., Fok, A. K., Allen, R. D., Gluck, S. L., Heuser, J. and Russell, D. G. (1994). Lack of acidification in Mycobacterium phagosomes produced by exclusion of the vesicular proton-ATPase. *Science* **263**, 678-81.

Swaim, L. E., Connolly, L. E., Volkman, H. E., Humbert, O., Born, D. E. and Ramakrishnan, L. (2006). Mycobacterium marinum infection of adult zebrafish causes caseating granulomatous tuberculosis and is moderated by adaptive immunity. *Infect Immun* **74**, 6108-17.

Swart, A. L., Harrison, C. F., Eichinger, L., Steinert, M. and Hilbi, H. (2018). Acanthamoeba and Dictyostelium as Cellular Models for Legionella Infection. *Front Cell Infect Microbiol* **8**, 61.

Temesvari, L., Zhang, L., Fodera, B., Janssen, K. P., Schleicher, M. and Cardelli, J. A. (2000). Inactivation of lmpA, encoding a LIMPII-related endosomal protein, suppresses the internalization and endosomal trafficking defects in profilin-null mutants. *Mol Biol Cell* **11**, 2019-31.

Triantafilou, M., Gamper, F. G., Haston, R. M., Mouratis, M. A., Morath, S., Hartung, T. and Triantafilou, K. (2006). Membrane sorting of toll-like receptor (TLR)-2/6 and TLR2/1 heterodimers at the cell surface determines heterotypic associations with CD36 and intracellular targeting. *J Biol Chem* **281**, 31002-11.

Tuxworth, R. I., Weber, I., Wessels, D., Addicks, G. C., Soll, D. R., Gerisch, G. and Titus, M. A. (2001). A role for myosin VII in dynamic cell adhesion. *Curr Biol* **11**, 318-29.

Vega, M. A., Rodriguez, F., Segui, B., Cales, C., Alcalde, J. and Sandoval, I. V. (1991). Targeting of lysosomal integral membrane protein LIMP II. The tyrosine-lacking carboxyl cytoplasmic tail of LIMP II is sufficient for direct targeting to lysosomes. *J Biol Chem* **266**, 16269-72.

Veltman, D. M., Keizer-Gunnink, I. and Haastert, P. J. (2009). An extrachromosomal, inducible expression system for Dictyostelium discoideum. *Plasmid* **61**, 119-25.

Vergne, I., Chua, J., Singh, S. B. and Deretic, V. (2004). Cell biology of mycobacterium tuberculosis phagosome. *Annu Rev Cell Dev Biol* **20**, 367-94.

Vicinanza, M., Di Campli, A., Polishchuk, E., Santoro, M., Di Tullio, G., Godi, A., Levtchenko, E., De Leo, M. G., Polishchuk, R., Sandoval, L. et al. (2011). OCRL controls trafficking through early endosomes via PtdIns4,5P(2)-dependent regulation of endosomal actin. *EMBO J* **30**, 4970-85.

Vishnyakova, T. G., Kurlander, R., Bocharov, A. V., Baranova, I. N., Chen, Z., Abu-Asab, M. S., Tsokos, M., Malide, D., Basso, F., Remaley, A. et al. (2006). CLA-1 and its splicing variant CLA-2 mediate bacterial adhesion and cytosolic bacterial invasion in mammalian cells. *Proc Natl Acad Sci U S A* **103**, 16888-93.

Westphal, M., Jungbluth, A., Heidecker, M., Muhlbauer, B., Heizer, C., Schwartz, J. M., Marriott, G. and Gerisch, G. (1997). Microfilament dynamics during cell movement and chemotaxis monitored using a GFP-actin fusion protein. *Curr Biol* **7**, 176-83.

Wilczynska, Z. and Fisher, P. R. (1994). Analysis of a complex plasmid insertion in a phototaxis-deficient transformant of Dictyostelium discoideum selected on a Micrococcus luteus lawn. *Plasmid* **32**, 182-94.

Yates, R. M. a. R., D. G. . (2008). Methods in Molecular Biology, vol. 445: Autophagosome and Phagosome Edited by: V. Deretic © Humana Press, Totowa, NJ, pp. 311-325.

Zhang, X. and Soldati, T. (2013). Detecting, visualizing and quantitating the generation of reactive oxygen species in an amoeba model system. *J Vis Exp*, e50717.

Zhang, X. and Soldati, T. (2016). Of Amoebae and Men: Extracellular DNA Traps as an Ancient Cell-Intrinsic Defense Mechanism. *Front Immunol* **7**, 269.

Zhang, X., Zhuchenko, O., Kuspa, A. and Soldati, T. (2016). Social amoebae trap and kill bacteria by casting DNA nets. *Nat Commun* **7**, 10938.

Figures

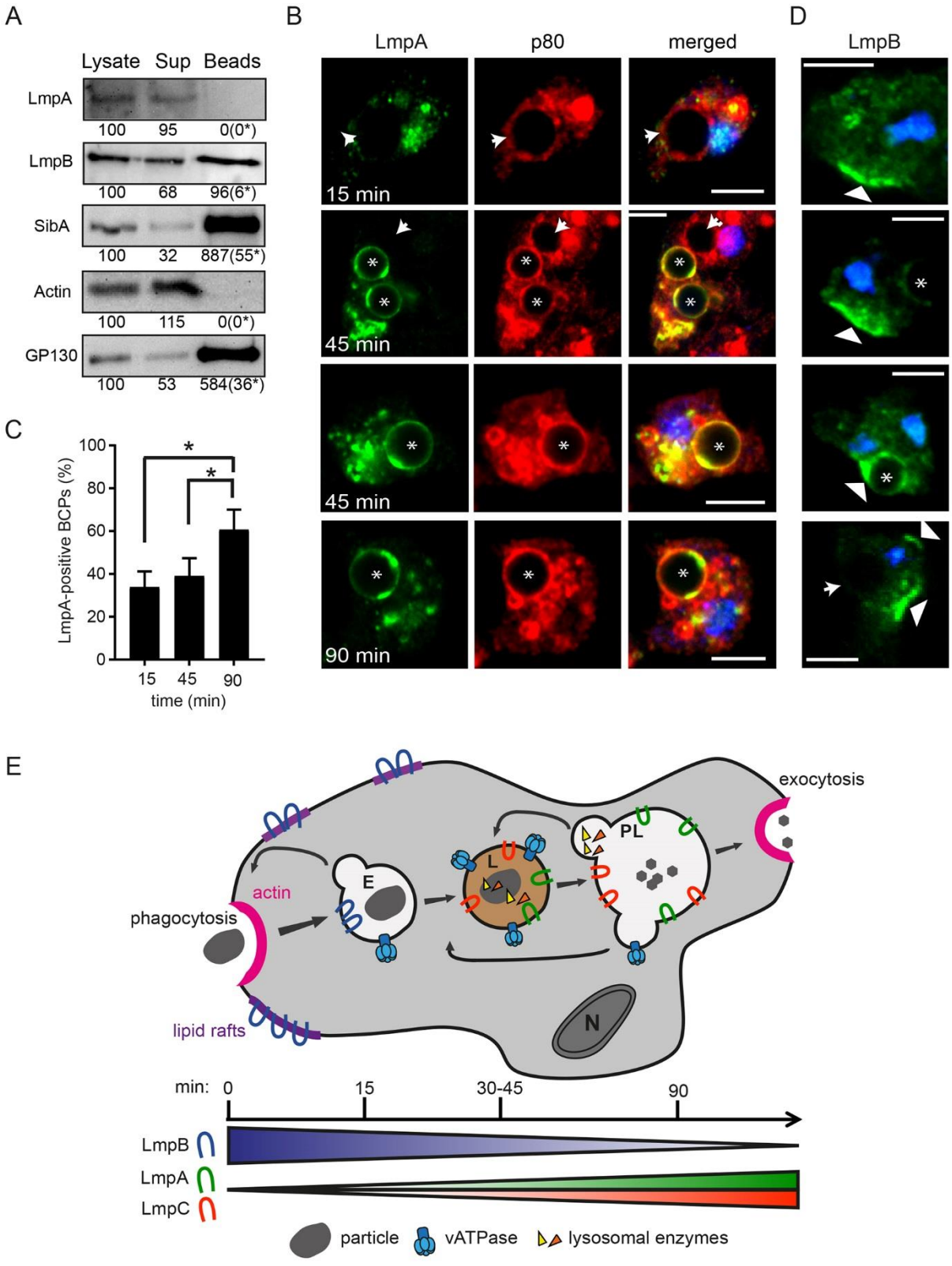

Fig. 1. LmpB is found at the plasma membrane and LmpA localizes at lysosomes and postlysosomes. **A.** Plasma membrane proteins of wt cells were biotinylated and isolated by pulldown with avidin beads. The lysate, supernatant (Sup) and bound (Beads) fractions were immunoblotted for known markers of the plasma membrane (SibA, GP130) or actin as a negative control. LmpB is enriched in the plasma membrane while LmpA is not present in the biotinylated fraction. Representative blots are shown, with quantifications of the signal intensity relative to the lysate fraction. The beads fraction was concentrated 16 times, number in brackets (*) indicates the corrected value (absolute value divided by 16). **B.** Confocal fluorescence microscopy of fixed *lmpA* kd cells expressing LmpA-FLAG phagocytosing 3 µm latex beads. At the indicated time points, cells were fixed and immunostained with an anti-FLAG antibody to detect LmpA-FLAG, and with anti-p80 to label endocytic compartments. Arrows indicate bead-containing phagosomes negative for LmpA; asterisks label LmpA-positive phagosomes. Scale bar, 5 µm. **C.** Quantification of B. Bars represent the mean and SD of three independent experiments (*p = 0.4712; unpaired t-test). Between 175 and 316 beads were analysed per time point. **D.** Confocal fluorescence microscopy of fixed *lmpB* ko cells expressing LmpB-FLAG phagocytosing 3 µm latex beads. Cells were fixed and immunostained with anti-FLAG antibody without permeabilization. Images representative for different uptake stages were chosen. **E.** Scheme representing the localization of LmpA, LmpB and LmpC throughout the phagosome maturation pathway. LmpB is in lipid rafts at the plasma membrane and early endosomes; LmpA and LmpC accumulate gradually in lysosomes and postlysosomes, as shown by us and others (Gotthardt et al., 2006a; Gotthardt et al., 2002). E, endosome; L, lysosome; PL, postlysosome: N, nucleus; brown colour, acidic pH.

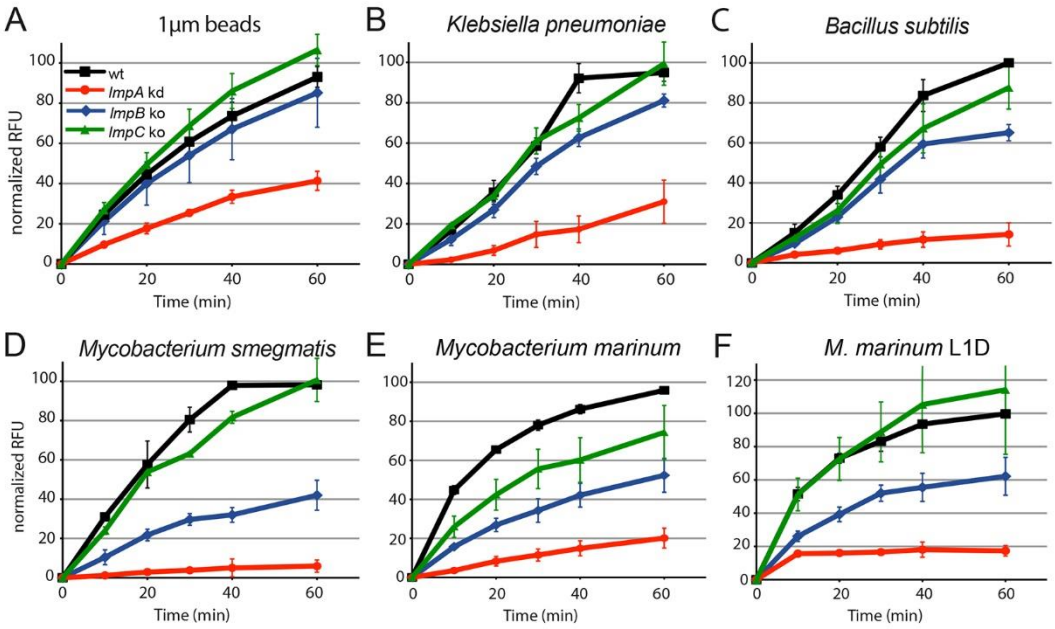

Fig. 2. The *lmpA* kd strain shows severe defects in phagocytosis. The uptake of different fluorescent particles [1 µm yellow-green (YG)-beads **(A)**, Alexa 488-labeled *K. pneumoniae* (**B**) and *B. subtilis* (**C**), and GFP-producing *M. smegmatis* (**D**), *M. marinum* wt (**E**) and *M. marinum* L1D (**F**)] by wt, *lmpA* kd, *lmpB* ko or *lmpC* ko cells was monitored by flow cytometry, and the mean and the standard error of the mean (SEM) of three to four independent experiments are represented. RFU were normalized to the fluorescence of wt cells after 60 minutes of uptake.

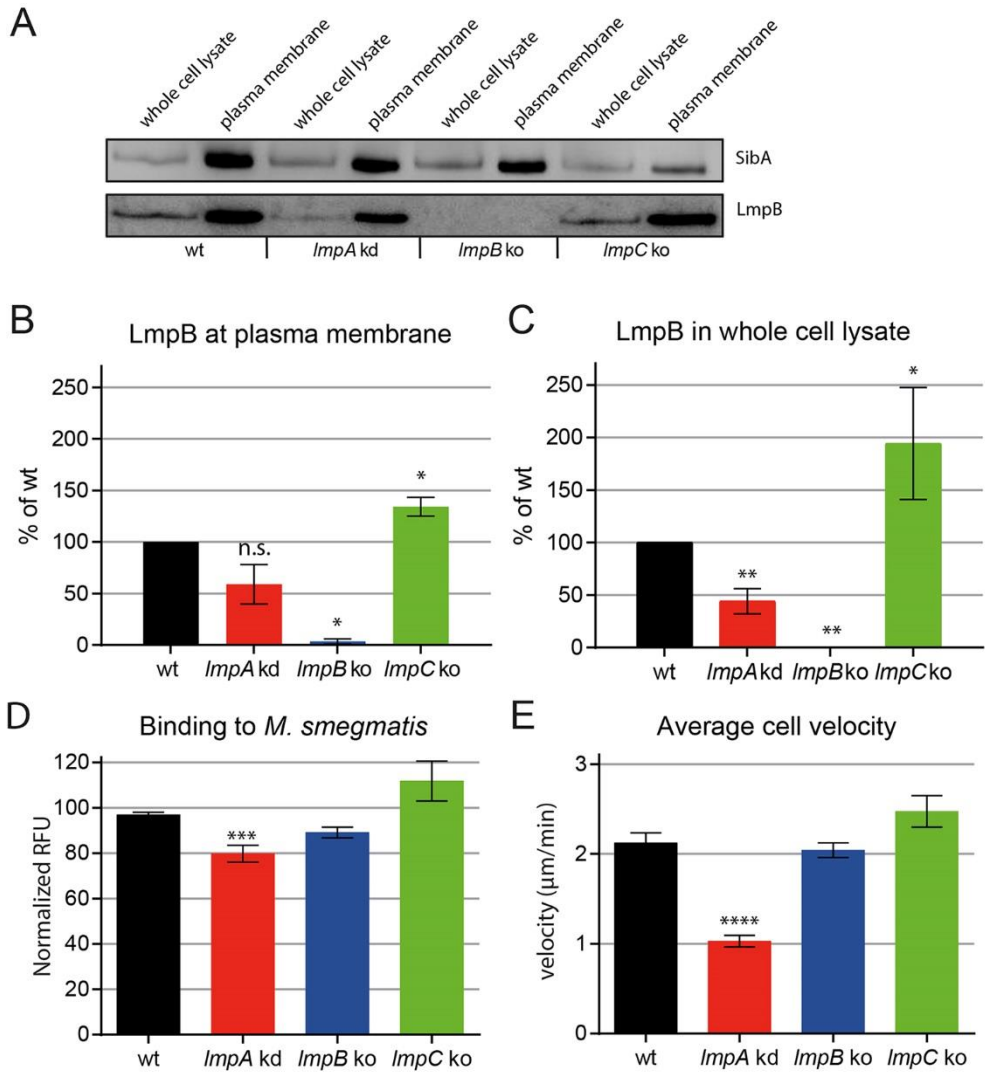

Fig. 3. *lmp*A kd cells have altered surface levels of LmpB, as well as adhesion and cellular motility defects. A-C. Biotinylated plasma membrane proteins from wt, *lmpA* kd, *lmpB* ko and *lmpC* ko cells were isolated on avidin beads and immunoblotted along whole cell lysates with anti-SibA and anti-LmpB antibodies. **A** shows one representative blot of three independent experiments. **B** and **C.** Quantification of the amount of LmpB at the plasma membrane (**B**) or in the whole cell lysate (**C**) of the different mutants compared to wt levels. Graphs indicate mean and SEM of 3 independent experiments (* $p \leq 0.05$, ** $p \leq 0.01$, Student's *t*-test). **D.** Adhesion of Syto9-labeled *M. smegmatis* to cells in cold medium containing sodium azide was monitored by flow cytometry after a mild PFA fixation. Graphs indicate mean and SEM of 2-4 independent measures from 3 independent experiments (***$p \leq 0.001$; Student's *t*-test) **E.** Average velocity of random cell motility for each strain. Graphs indicate the mean and SEM of three independent experiments (****$p \leq 0.0001$; Student's *t*-test).

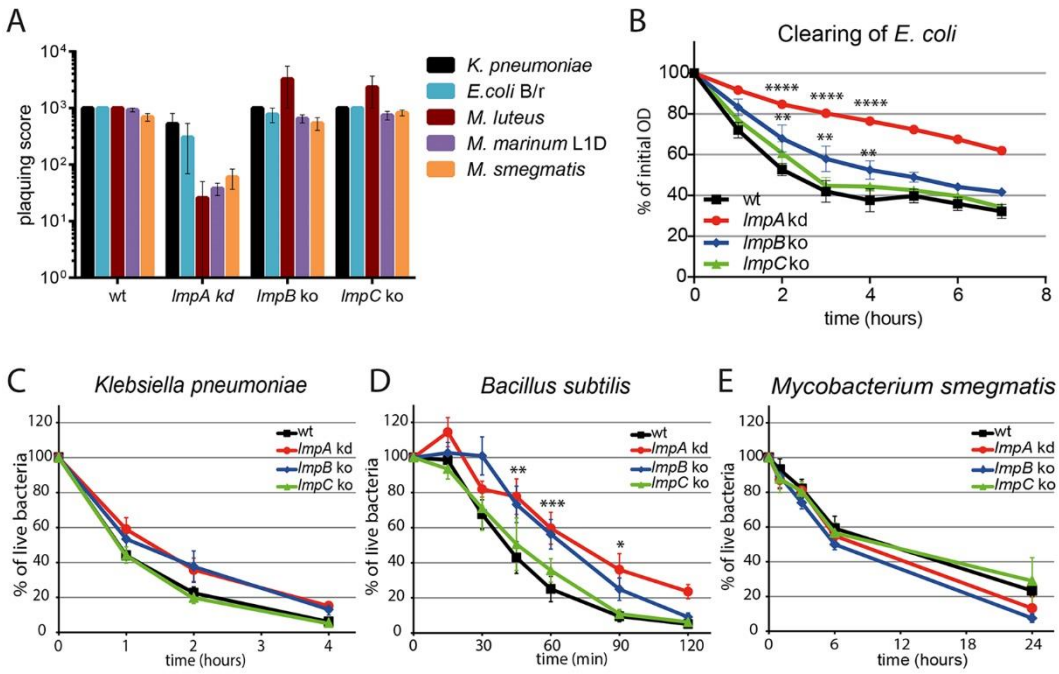

Fig. 4. Growth on diverse bacteria, but not killing, is affected in *lmpA* kd cells. A. Plaquing score of wt, *lmpA* kd, *lmpB* ko or *lmpC* ko cells on various bacteria. 10, 10^2, 10^3 or 10^4 cells of each *D. discoideum* strain were deposited on bacteria lawns. Plaquing was quantified using a logarithm score (see Materials and Methods). Graph indicates the mean and SEM of 3 to 22 independent experiments. **B.** Clearing of heat-killed *E. coli* by wt, *lmpA* kd, *lmpB* ko or *lmpC* ko cells over 7 hours monitored by OD_{600} measurements at the indicated time points. Curves indicate the mean and SEM of three independent experiments. **C-E.** Killing of various bacteria by wt, *lmpA* kd, *lmpB* ko or *lmpC* ko. **C** and **D.** Cells were incubated with *K. pneumoniae* and *B. subtilis*, and the number of surviving bacteria at the indicated time points was determined by cfu counting after lysing the cells and plating the lysates on LB agar plates. **E.** Cells were spinoculated with FFluc-expressing *M. smegmatis*. At the given time points, the infected cells were lysed, the released bacteria were incubated with luciferin, and luminescence was measured with a plate reader. Curves represent the mean and SEM of 4 to 6 independent experiments done in duplicates or triplicates (* $p \leq 0.05$, ** $p \leq 0.01$, *** $p \leq 0.001$, **** $p \leq 0.0001$; two-way Anova and Bonferroni post-hoc test).

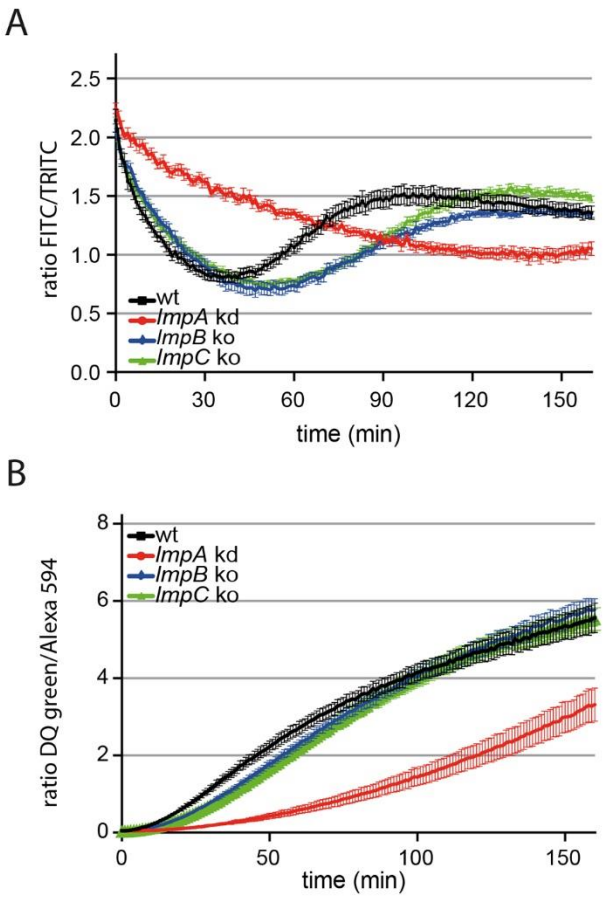

Fig. 5. Phagosome acidification and proteolysis are strongly perturbed in *lmpA* kd cells. A and B. Phagosomal acidification and proteolysis measured in wt, *lmpA* kd, *lmpB* ko and *lmpC* ko strains. **A.** Cells were spinoculated together with silica beads coupled to the pH-sensitive FITC and the pH-insensitive TRITC. Differences in fluorescence emission due to pH changes were measured with a fluorescence plate reader, and the FITC/TRITC emission ratios were calculated. **B.** Cells were spinoculated with silica beads coupled to the self-quenching reporter DQ Green and the reporter dye Alexa 594. Digestion of BSA causes dequenching of DQ Green and an increase in its fluorescence. The graph is plotted as the ratio of DQ Green/Alexa 594 emission as a function of time. Curves of **A.** and **B.** represent the mean and SEM of 8 to 10 measurements from 5 independent experiments.

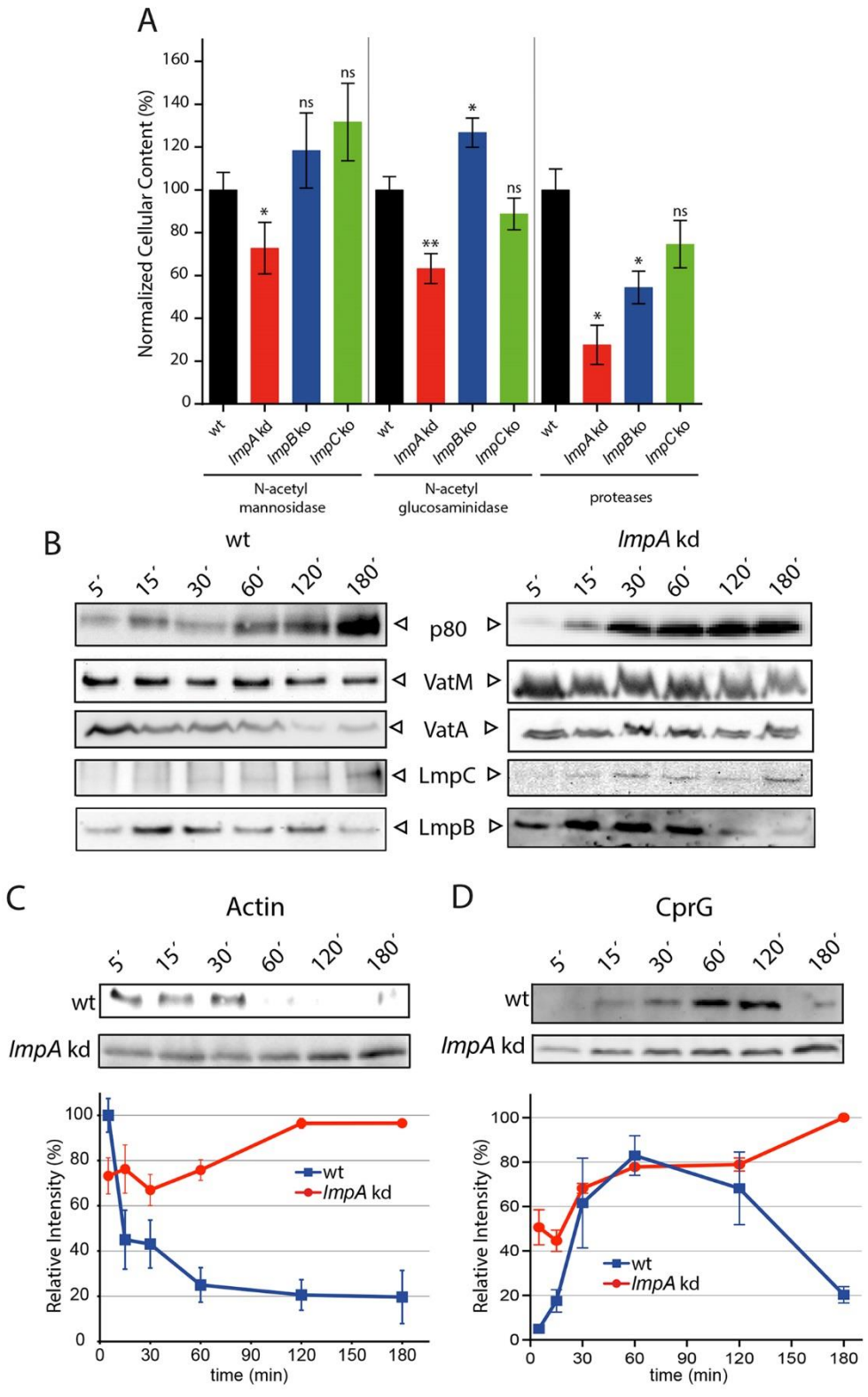

Fig. 6. Total hydrolytic enzymes activity and maturation of purified phagosomes. A. The total content of the N-acetyl-glucosaminidase and N-acetyl-mannosidase lysosomal enzymes in wt, *lmpA* kd, *lmpB* ko and *lmpC* ko cells was measured with an ELISA microplate reader after incubating cell lysates with the respective chromogenic substrates. The activity of proteolytic enzymes was assessed with silica beads coupled to the self-quenching reporter DQ Green-BSA and the reference dye Alexa 594 in K-acetate buffer (pH 4). Graphs indicate the mean normalized to wt and SEM of 3 to 4 independent experiments performed in up to technical sextuplicates (* $p \leq 0.05$, ** $p \leq 0.01$, two-tailed Student's *t*-test). **B**, **C and D.** Phagosome maturation in wt and *lmpA* kd cells. Phagosomes containing latex beads were purified, and specific proteins were monitored by quantitative immunoblotting as described previously (Gotthard 2006b). **B.** Representative blots of VatM, VatA, p80, LmpB or LmpC between phagosomes from wt and *lmpA* kd cells. **C and D.** Representative blots and the corresponding quantifications of two independent experiments for actin and CprG demonstrating differences in their maturation profiles in the *lmpA* mutant. Graphs indicate mean and SEM.

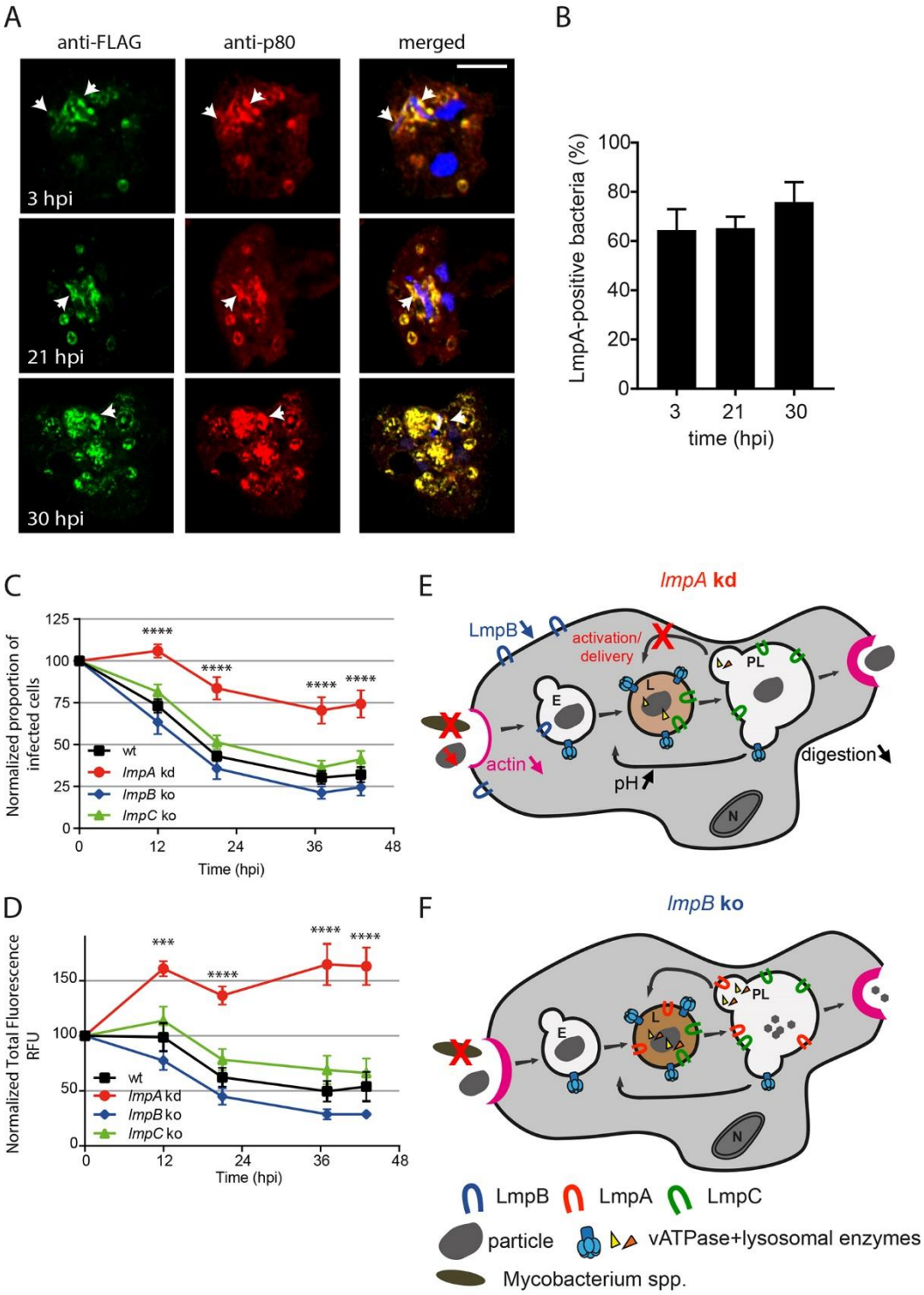

Fig. 7. LmpA localizes to the MCV and *lmpA* kd cells are more susceptible to infection with *M. marinum* than wt cells. A. LmpA-FLAG localisation during infection. Cells expressing LmpA-FLAG were infected with unlabelled *M. marinum*. At the indicated time points, cells were fixed and antibodies against p80 and FLAG were used to label the MCV and to detect LmpA-FLAG, respectively. Scale bar, 5 µm. **B.** Quantification of **A**. No statistical significance was observed between the time points (unpaired t-test). Bars

represent the mean and SD of three independent experiments. At least 70 MCVs were quantified per time point. **C** and **D**. *M. marinum* infection dynamics in wt, *lmpA* kd, *lmpB* ko and *lmpC* ko cells. Cells were infected with GFP-producing *M. marinum* by spinoculation. Samples were taken at the indicated time points, and the dynamics of infection were monitored by flow cytometry. Representative SSC vs FL1 plots are presented in Fig. S4. Graphs indicate mean and SEM of 9-10 independent experiments (*** $p \leq 0.001$, **** $p \leq 0.0001$; two-way Anova and Bonferroni post-hoc test). **E.** and **F.** Working model of the *lmpA* kd and *lmpB* ko phenotypes. *lmpA* kd cells has reduced levels of LmpB, defective particle uptake due to impaired actin-dependent processes and decreased lysosomal biogenesis (**E.**); *lmpB* ko cells are specifically impaired in *Mycobacterium* spp. uptake (**E.**). E, endosome; L, lysosome; PL, postlysosome; N, nucleus.

Table 1. List of phenotypes of the different cell lines

Phenotypes		***lmpA* kd**	***lmpB* ko**	***lmpC* ko**
Phagocytosis (Fig. 2)	Beads	< wt	= wt	= wt
	K. pneumoniae	< wt	= wt	= wt
	B. subtilis	<< wt	< wt	= wt
	Mycobacteria	<< wt	< wt	= wt
LmpB levels (Fig. 3A-C)		**PM:** < wt **Total:** < wt	/	**PM:** > wt **Total:** > wt
Adhesion to *M. smegmatis* (Fig. 3D)		< wt	= wt	= wt
Motility (Fig. 3E)		< wt	= wt	= wt
Clearing of *E. coli* (Fig. 4B)		<< wt	< wt	= wt
Killing (Fig. 4C-E)	*K. pneumoniae*	= wt	= wt	= wt
	B. subtilis	< wt	< wt	= wt
	M. smegmatis	= wt	= wt	= wt
Acidification (Fig. 5A)		pH > wt neutralization delayed	pH = wt neutralization delayed	pH = wt neutralization delayed
Proteolysis (Fig. 5B)		< wt	= wt	= wt
Cellular content lysosomal enzymes (Fig. 6A)	N-acetyl mannosidase	< wt	= wt	= wt
	N-acetyl glucosaminidase	< wt	> wt	= wt
	Proteases	<< wt	< wt	= wt
Actin on phagosome (Fig. 6C)		> wt	/	/
CprG on phagosome (Fig. 6D)		delayed	/	/
Infection (Fig. 7C and D)		**% infected cells:** > wt **Total Fluo:** > wt	**% infected cells:** = wt **Total Fluo:** = wt	**% infected cells:** = wt **Total Fluo:** = wt

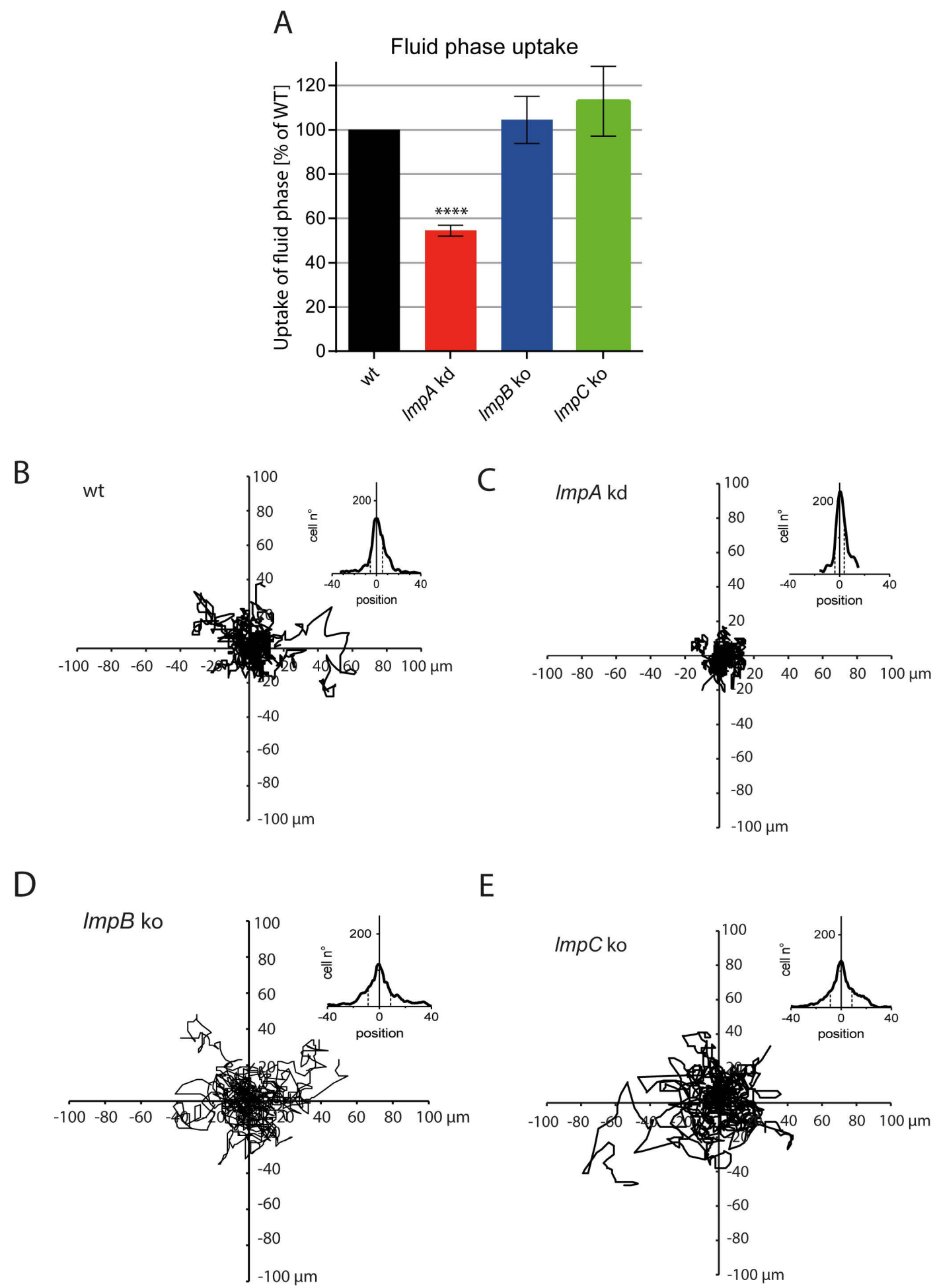

Sup Fig. 1. Fluid phase uptake and random motility of wt, *lmpA* kd, *lmpB* ko, *lmpC* ko cells. A. To measure the fluid phase uptake, cells were incubated 20 minutes with Alexa 647-coupled dextran, and the internalized fluorescent signal was measured by flow cytometry and expressed as the percentage of the levels in wt cells. Graphs depict the mean and SEM of four independent experiments. **B-E.** Cells were plated in medium onto a glass slide and their random cell motility was monitored every 30 seconds for 60 minutes. Metamorph Office software was used for cell tracking. Shown are representative experiments with tracks of 20 cells each, aligned at origin. The distribution of all cell positions around the origin corresponds to a Gaussian distribution, shown in the upper right corner of each graph.

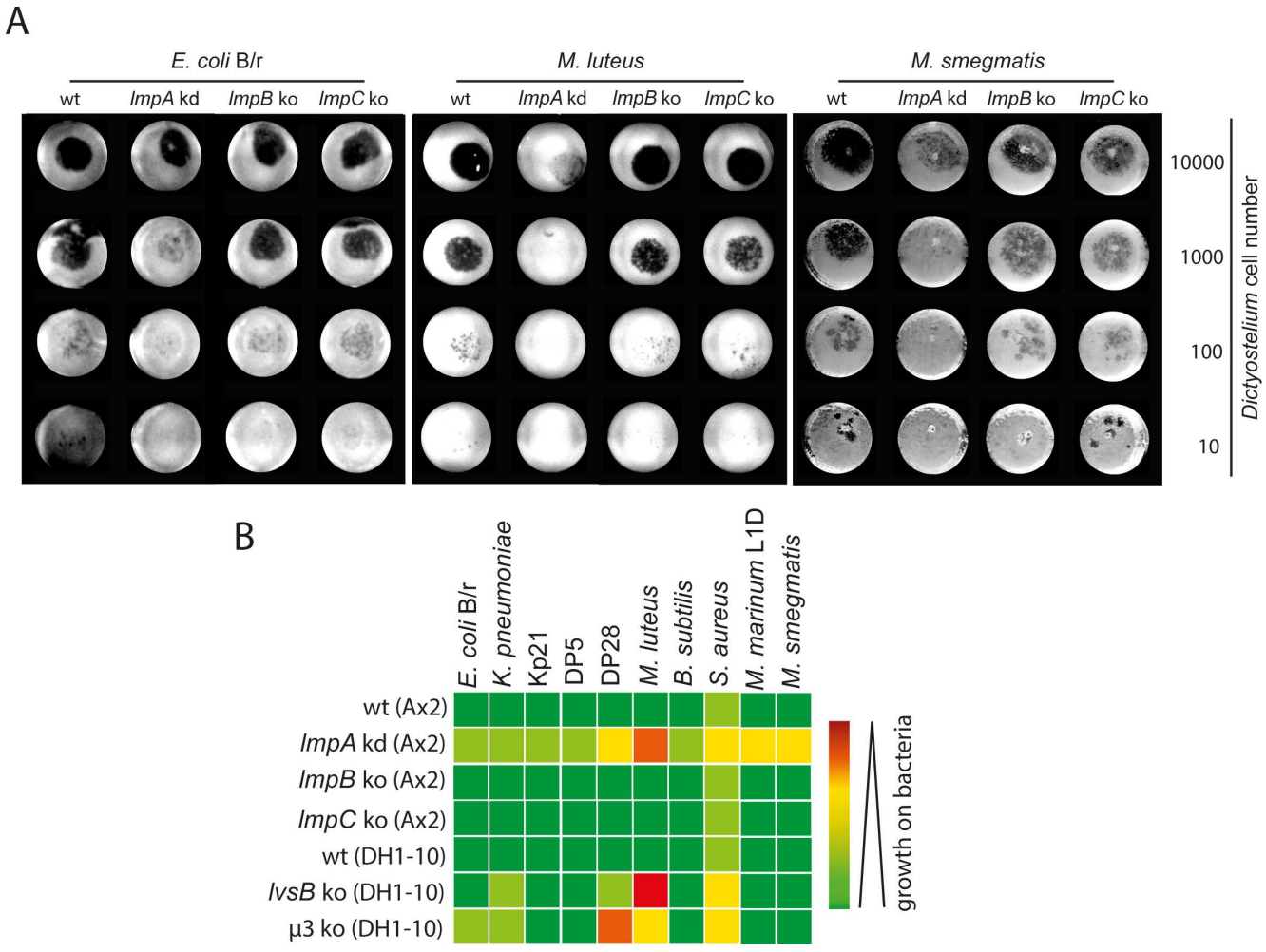

Sup Fig. 2. Growth of *lmp*A kd, *lmpB* ko and *lmpC* ko cells on diverse bacteria. A. 10, 10^2, 10^3 or 10^4 cells of either *D. discoideum* wt, *lmpA* kd, *lmpB* ko or *lmpC* ko were deposited on a lawn of various bacterial strains. Representative images are shown for *E. coli*, *M. luteus* and *M. smegmatis*. **B.** Colour-coded summary of 3 to 22 plaque formation experiments. Plaque formation up to a dilution of 10, 10^2, 10^3 or 10^4 cells is indicated in dark green, light green, yellow and red, respectively.

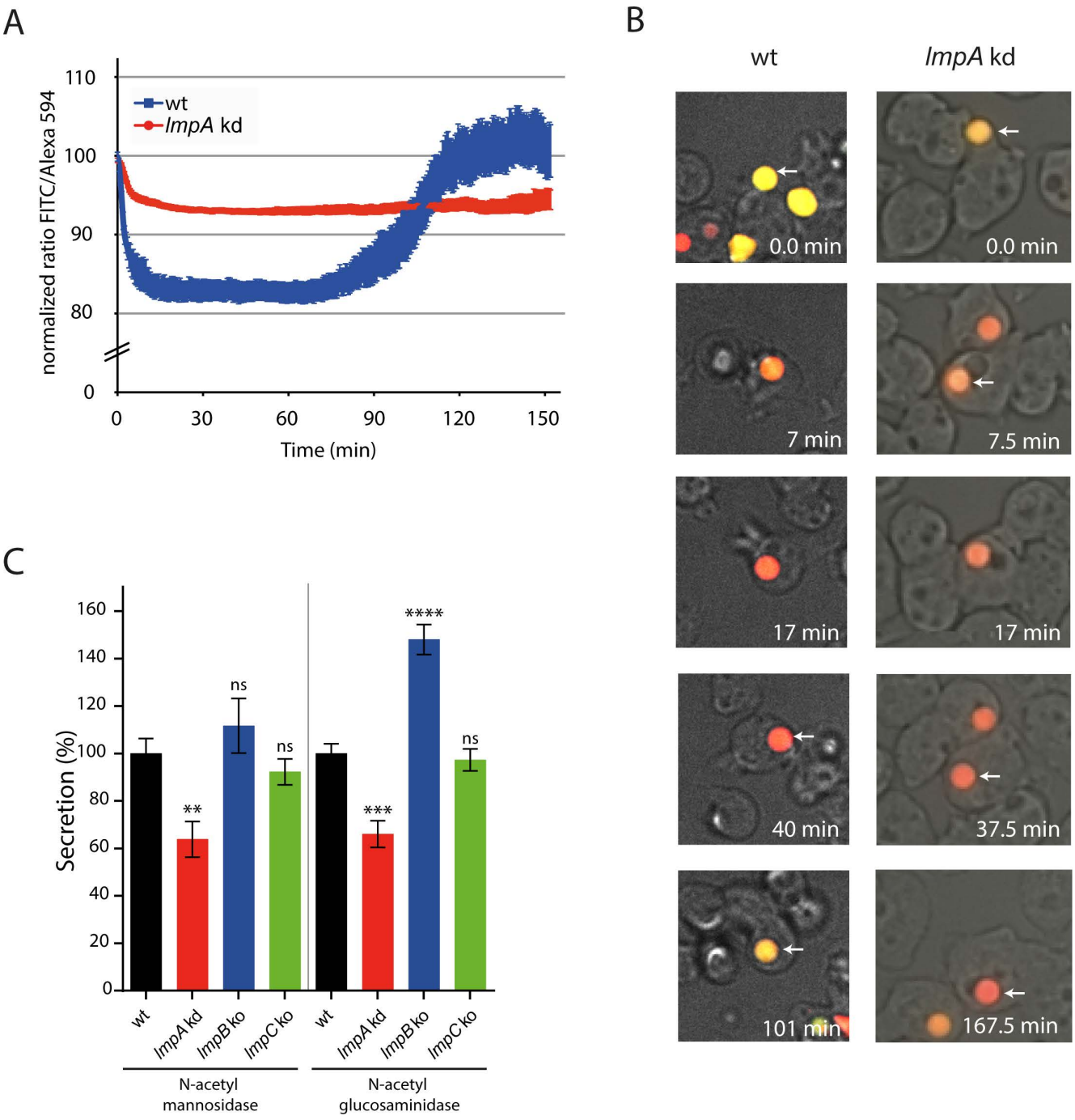

Sup. Fig. 3. Acidification and secretion of lysosomal enzymes are strongly perturbed in *lmpA* kd cells.

A and **B.** Acidification of single phagosomes measured by live microscopy. wt and *lmpA* kd cells were incubated with silica beads coupled to FITC and Alexa 594, and fluorescence emission was measured live for three hours. **A.** Graphs show the mean and SEM of 13 to 23 beads from 2 to 3 independent experiments per cell line normalized to time zero. **B.** Snapshots from two movies showing the fluorescence transitions of FITC/Alexa 594-labeled beads; yellow colour, neutral pH; red colour, acidic pH **C.** Secretion of lysosomal N-acetyl-glucosaminidase and N-acetyl-mannosidase enzymes measured in wt, *lmpA* kd, *lmpB* ko and *lmpC* ko. Cells were incubated for 6 hours in Hl5 medium and their supernatant was incubated in an ELISA microplate reader with their respective chromogenic substrates. Graphs indicate the mean normalised to wt and SEM of 3 independent experiments performed in up to technical sextuplicates (** $p \leq 0.01$, *** $p \leq 0.001$, **** $p \leq 0.0001$; Student's *t*-test).

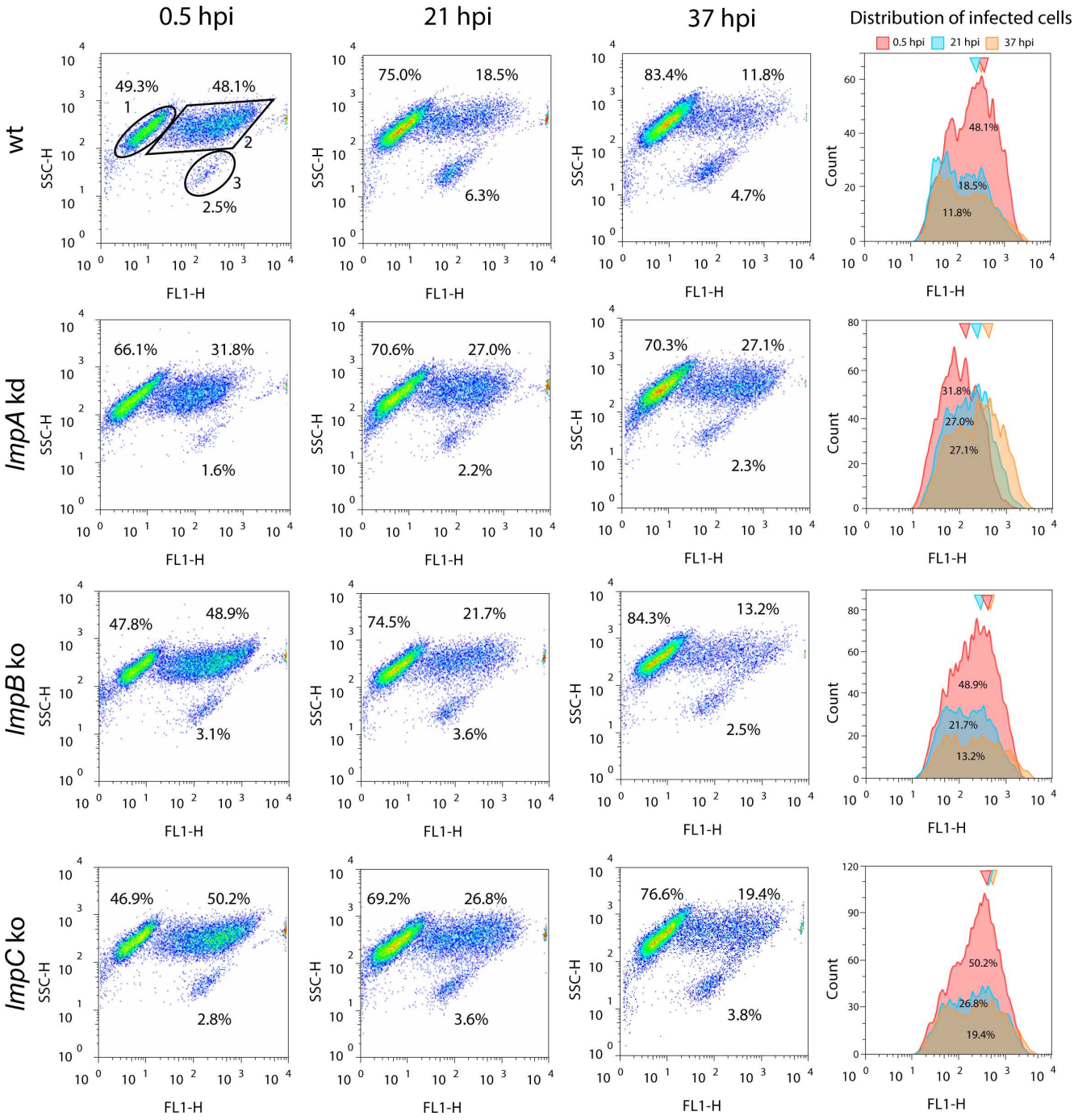

Sup. Fig. 4. *lmpA* kd cells are heavily infected by *M. marinum*. wt, *lmpA* kd, *lmpB* ko and *lmpC* ko cells infected with GFP-producing *M. marinum* were analyzed by flow cytometry. Plotting the side scatter (SSC) as a function of fluorescence (FL1) revealed three populations: (1) non-infected cells, (2) infected cells and (3) fluorescent extracellular bacteria, with the percentage of events in each gate shown. The fluorescence of the population of infected cells over time is also plotted, with the percentage of infected cells on each histogram as well as arrowheads depicting the mean fluorescence at each time point. At 0.5 hours post infection (hpi) all strains had a similar percentage of infected cells. While the proportion of infected wt, *lmpB* and *lmpC* cells decreased until 37 hpi, *lmpA* kd cells showed a higher degree of infection. In addition, *lmpA* kd infected cells, in contrast to the other cell lines, show an increase in fluorescence over time, suggesting that cells have a higher bacterial load.